Energy sustainability in the transport sector using synthetic fuels in series hybrid trucks with RCCI dual-fuel engine

Antonio García, Javier Monsalve-Serrano*, Rafael Lago Sari and Santiago Martinez-Boggio

CMT - Motores Térmicos, Universitat Politècnica de València, Camino de Vera s/n, 46022 Valencia, Spain

Fuel

Volume 308, 15 January 2022, 122024

https://doi.org/10.1016/j.fuel.2021.122024

Corresponding author (*):
Dr. Javier Monsalve-Serrano (jamonse1@mot.upv.es)
Phone: +34 963876559
Fax: +34 963876559

Abstract

The green-deal carbon neutrality target set for 2050 and CLOVE consortium predictions of NOx reductions confirm the efforts of the European commission to achieve a clean and sustainable transportation. In this sense, several solutions are needed to fulfill with the short-term regulation requirements and provide a sustainable transportation transition. This work assesses the potential and challenges of using a Reactivity Controlled Compression Ignition, RCCI, engine in a series hybrid medium duty truck fueled with both conventional and synthetic. The numerical results enabled to design the hardware and control system of the concept. Experimental results show a good agreement with numerical simulation estimation with CO_2 tailpipe below 3%. Overall, using diesel and gasoline, it is possible to fulfill the current EUVI regulation without after-treatment while promoting benefits of more than 10% in CO_2 Tank-to-Wheel emissions. The use of Oxymethylene Dimethyl ethers, OMEx, instead of diesel allows further reductions of both NOx and soot emissions due to its no carbon-to-carbon bonds and higher oxygen content. The Well-to-Wheel CO_2 analysis shows that OMEx-Gasoline operating as series hybrid achieves above 25% of CO_2 benefits against current commercial truck.

Keywords

Sustainability; Energy Transition; RCCI; Hybrid powertrain; Driving cycles

1. Introduction

Emissions restrictions suppose a huge challenge for the medium and heavy-duty transportation sector. Additionally, mandates were recently introduced requiring to reduce the Tank-to-Wheel (TTW) CO_2 emissions. In this scenario, pure electric vehicles appear as immediate solution [1]. However, the improvement in terms of Well-to-Wheel (WTW) and Life Cycle Analysis (LCA) CO_2 emissions are not evident compared to Internal Combustion Engines (ICE) or hybrids in the medium- and heavy-duty sector. In addition, due to the large energy requirements, the battery packs are large and expensive [2]. The current charging infrastructure is still limited to small regions and recharge times are still long [3]. In this sense, mid-term solutions are needed to fulfill with the short-term regulation requirements and provide a sustainable transportation transition. Hybrid powertrains appears a potential solution to fill this gap [4]. However, notable improvements in terms of maximum brake thermal efficiency, powertrain energy management, components cost and pollutant emissions need to be done [5].

The use of advanced combustion modes is pointed as a promising alternative to enable the pollutant reductions required [6]. Among the different advanced combustion modes that have been proposed along the years, the Reactivity Controlled Compression Ignition (RCCI) showed advantages in terms of combustion controllability and load range extension [7][8]. In spite of that, the concept stills suffers from low combustion efficiency at low engine loads and high-pressure gradients at high load, which limits its applicability to only part of the engine map [9]. These issues have encouraged the development of alternatives that enabled to keep the benefits of the RCCI combustion while covering the full engine maps [10]. In this sense, the dual-mode dual-fuel (DMDF) combustion concept has appeared as a promising solution, demonstrating to be capable of reducing the engine-out NOx emissions under the EUVI limits while delivering fuel consumption savings with respect to the conventional diesel combustion (CDC) and ultra-low soot emissions [11].

In spite of the benefits of using the DMDF or the RCCI concept, the CO_2 reductions that can be attained are still far from the limits proposed for the 2025 and 2030 scenarios [12]. Therefore, alternatives are required to enable further reductions of CO_2 while benefiting from the clean combustion process obtained with the dual-fuel combustion. Among the different strategies to reduce the CO_2, both electrification [13] and the use of synthetic fuels [14] are referred as promising technologies to be used. The former comprises technologies addressing mild hybrid hybridization as Belt Starter Assistance (BAS) [15] up to high hybridization degrees in parallel and series architectures [16]. In addition, the electric machine boosting mode in hybrid vehicles allows to reduce the internal combustion engine size or de-rating it. Garcia et al. [17] showed the possibility to move from a DMDF to a full RCCI engine with the electrification of the powertrain. In the above-mentioned work, the authors demonstrated the potential of using both RCCI and parallel hybridization for heavy-duty trucks, allowing to achieve reductions up to 15 % in CO_2 emissions in a TTW and fulfill the EUVI limits considering tailpipe values of NOx and soot emissions [18]. However, the real application of the concept may be hindered by the difficulties in achieving proper transient operating due to the significant gradients in the air management and injection settings from point-to-point. Therefore, the powertrain architectures that allow to operate the thermal engine at steady-state points or with the minimum level of transient may benefit the utilization of the RCCI combustion. Such conditions can be attained by combining the RCCI combustion concept with the series hybrid architecture.

The series hybrid architecture is the simplest form of Hybrid Electric Vehicle (HEV) architecture due to the decoupling of the ICE to the wheels. Both engine control and maintenance are easy and straightforward when compared to other HEV architectures. The thermal engine works solely as a power source for a generator, allowing it to be entirely decoupled from the vehicle speed and therefore operate at its peak efficiency point [19]. In addition, it avoids the transient operation found with conventional or parallel hybrid powertrains. Therefore, it is suitable to be applied with advance combustion modes, where the number of parameters to be optimized and modify in different operating points change drastically [20]. The main drawback of this concept is the amount of electric losses due to the passage of all the ICE energy to the generator and traction motor. In buses and trucks, this point is crucial due to the large power that is transferred to the wheels and generated in the engine. A significant constraint for the control logic of a series hybrid can be the noise, vibration, and harshness (NVH). Therefore, the optimization of the powertrain is a key task to the increase the global powertrain efficiency and make like current conventional powertrains. Several investigations evaluated the use of the series hybrid technology in trucks from the heavy-duty transportation sector [21] and buses [22]. The studies show that are particularly suitable for some specific applications such as urban buses, urban garbage collector trucks, and door to door delivery vans, which all have frequent stops and can benefit from decoupling the ICE from traction (operating in the highest brake thermal efficiency) as well as from regenerative braking (due to the high mass of the vehicle and the frequent stops in this urban conditions). However, all of them are based in conventional diesel combustion and no one studies the use of advanced combustion modes or synthetic fuels.

Alternative fuels, as synthetic fuels derived from green energy sources, have the potential to reduce the Well-to-Wheel CO_2 emissions due to the low Well-to-Tank (WTT) emissions associated to their production processes [23]. These fuels offer an additional degree of CO_2 reduction since they combine the use of this emission as raw material, together with renewable energy, to obtain a wide range of molecules that can be burn in conventional internal combustion engines [24]. Depending on the production process, fuels as methanol, synthetic gasoline and e-Fischer Tropsch [25] can be obtained. Other fuels as Oxymethylene Dimethyl Ethers can be attained from further processing of methanol [26]. Recently, OMEx was identified as a potential fuel to mitigate the soot formation in both conventional diesel combustion and also RCCI combustion due to its high oxygen concentration and the absence of carbon-to-carbon bonds [27]. This effect provides an additional degree of freedom to optimize the engine efficiency and reduce the NOx emissions at the same time. The combination of synthetic fuels such as OMEx with advanced combustion modes in hybrid applications may offer the required solution to the short- and mid-term transport decarbonization requirements, enabling to follow the proposed path to a carbon neutrality in 2050 [28]. Despite of their potential, no investigation addresses in detail the benefits and challenges that may be attained in combining these technologies concerning energy conversion, efficiency, emissions and real implementation [29].

Therefore, this work aims to demonstrate the benefits of using the RCCI combustion mode in a series hybrid with conventional and synthetic fuels in order to find alternatives to push the energy transportation sustainability. Steady-state experimental engine calibration was carried out to feed the vehicle models. Later, experimental transient tests are performed to understand the accuracy of the emissions predictions. Lastly, OMEx-gasoline steady-state calibration is used to optimize the series hybrid powertrain and find the best setup. The results are compared to the diesel-gasoline series hybrid case and the current commercial diesel non-hybrid truck. Thus, this is a one-of-a-kind study, evaluating by the first time the extension of the Dual-Mode Dual-Fuel combustion in experimental transient applications, representative of a series hybrid truck. In addition, the work proposes a comparison with 0-D simulations as a validation step but also a database to developed refined models to account the specificities of the combustion concept for enhanced modelling. Finally, considering the outcomes of the previous investigations, the potential of the series-hybrid platform in reducing criteria pollutants and CO_2 emissions is assessed for both conventional and synthetic fuels.

2. Methodology

The evaluation of a truck platform representative of medium-duty applications using RCCI LTC combustion mode was performed in a 0-D numerical vehicle model. The new concept proposed is a series hybrid powertrain with a de-rated 8L six-cylinder engine adapted to operate in RCCI mode. Experimental engine calibration in stationary conditions and transient cycles to validate and feed the numerical model were performed. The results are compared against the non-hybrid commercial powertrain in CDC and DMDF mode to understand the advantages and drawback against current commercial technology and the proposed in the past by the research group [11]. The methodology applied to design, test, validate and post-process the results is explained in the next subsections.

2.1. Numerical vehicle model

The 0-D vehicle model was developed in the GT-Suite® commercial software (v2021, Gamma Technologies) modifying the non-hybrid model by adding the new powertrain components [30]. The numerical model used in this investigation is an evolution of previous models presented by the author in different works [9]. It is worth to mention that these models were fully validated regarding fuel consumption and emissions for real driving conditions as presented in [31]. For each time step, the model calculates the require torque and engine speed to fulfil with the required vehicle velocity from the driving cycle. The values of engine speed and torque (BMEP) are used as inputs to the experimental maps that are loaded in the model to determine the instantaneous production of fuel consumption and emission by means of map interpolation. More details and a complete description of the numerical methodology are presented in GT drive manual [32]. The truck is a Volvo FL 18-ton maximum payload representative of the European medium-duty sector for goods transportation in urban and extra-urban conditions. This truck is originally equipped with an 8L six-cylinder diesel engine with a maximum power of 280 hp. It uses an after-treatment system (ATS) system composed of a SCR-urea (NOx reduction) [33], DOC (HC and CO reduction) [34] and DPF (soot filtration) [35] for achieving the current EUVI normative [36]. In the current work, the original engine was modified to enable the dual-mode dual-fuel operation. Results from previous investigations demonstrated that this concept can use a fully premixed RCCI combustion with ultra-low NOx and soot up to 60 % of engine load (210 hp brake output). Therefore, for the hybrid series powertrain, the engine is de-rated to 60% of engine load, thus avoiding the upper part of the map in which the emissions levels increase [24].

As the main constraint for the hybrid powertrain design is to achieve at least the same performance than the commercial truck (maximum power and torque output), the traction motor is designed with the same maximum power output than the CDC ICE (280 hp). A second electric machine is coupled to the ICE to operate as generator. Therefore, the maximum power output of this electric machine (EM) is 210 hp. Both electric machines are modeled with efficiency maps and the maximum torque output against the rotational speed that is set. A scheme of the proposed powertrain is shown in Figure 1. The battery package is composed of several cylindrical lithium-ion modules (parallels and series cells) to achieve 600 V. The battery size (energy content) is optimized in the results sections by means of a design of experiments (DoE). The battery cells are modeled with an equivalent Thevenin model calibrated with experimental results from data of A123 cylindrical cells of 2.5 Ah, 3.3 V and 72 g (9.48 kg/kWh). It was selected a wide range of battery capacity to understand the effect in fuel consumption and emissions. The model is tested with a battery from 20 kWh to 80 kWh. The minimum is selected to be able to feed the traction motor and the generator at maximum power. The maximum is close to a light duty pure electric vehicle and half of size of a pure electric heavy-duty vehicle. This means an addition of extra weight compared to the conventional powertrain, 228 kg and 911 kg considering 20% extra for casing and cabling, respectively. Lastly, this concept needs two fuel tanks. As demonstrated in previous work [37] , this calibration work close to 50/50 Diesel and Gasoline and with similar total mass fuel consumption. So, for the case of conventional fuels the original tank can be divided in two parts and no extra weight it is necessary. For the case of OMEx-Gasoline due to the low LHV of OMEx the mass consumption will increase. Therefore, the HRF tank need to be increased. With the results obtained in this work it is possible to size the new fuel tank. More information about the electrical components models can be seen in [17].

The main advantage of this hybrid architecture is decoupling the ICE from the wheels. Therefore, the ICE speed and load can be set independently on the road conditions. This is especially advantageous for advanced combustion modes as RCCI due to the simplification of the transient regime. The generator can send the energy generated to the battery pack or directly to the traction motor when high power requirements are needed. This last point decreases the electric losses in the battery pack. The regenerative braking is one of the key aspects that needs to be considered and studied when a hybrid electric vehicle is under evaluation. The series hybrid braking system retains all the major components of the conventional mechanical brakes and adds the electric machine braking torque on the rear axle. The rear brakes in a truck cannot deliver the 100% of the power during a deceleration phase. The Economic Commission of Europe (ECE) stablishes a brake regulation, which indicates the minimum braking force on the rear wheels. In this work an optimum braking split between the rear and front wheels which is known as I-Curve [38] that meets the legislation requirements and improves the regenerative braking was used. This gives the maximum braking force that makes the front and rear wheels lock simultaneously in each friction coefficient. When the braking force is distributed to the front and rear wheels on the I-Curve, safe braking is assured. For this truck the I-Curve distribution is around 65% for rear axles and 35% for the front axles. Additional limitation in the braking system is added as battery maximum power and SOC limitation for the battery safe. In addition, below 5 km/h the truck does not recover energy due to a safety limitation. This sub model is included in GT-SUITE truck model and linked to the electric machine and mechanical brakes.

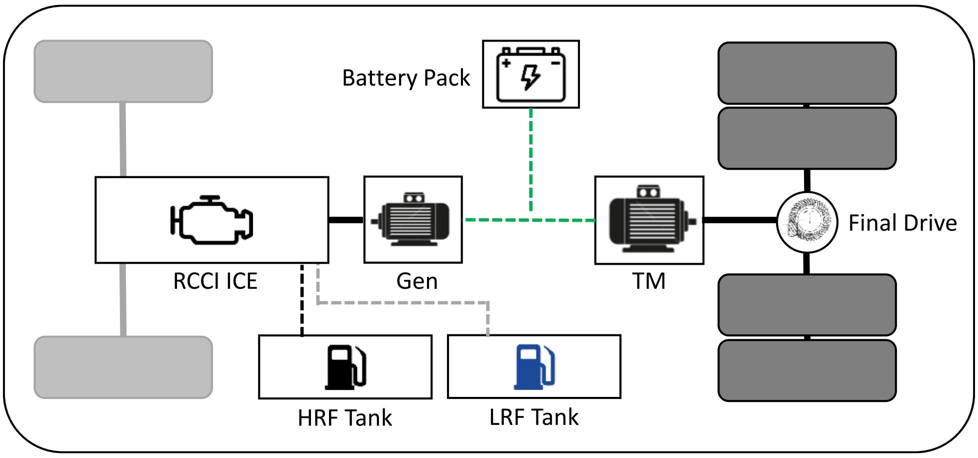

Figure 1 – Series Hybrid RCCI Truck concept. RCCI ICE (Reactivity Controlled Compression Ignition Internal Combustion Engine), Gen (Electric Motor Generator), TM (Traction Motor), HRF (High Reactivity Fuel) and LRF (Low Reactivity Fuel).

2.2. Experimental facility description

An active dynamometer is used for steady-state engine calibration and transient test (Figure 2). As it can be observed, different sensors were included to monitor and acquire variables of interest. The in-cylinder pressure was measured by means of Kistler 6125C pressure sensors. These signals were processed in a real-time by means of a heat release analysis routine built in LabVIEW, enabling the real-time visualization of the main combustion metrics such as combustion duration, combustion phasing, among others. The temporal signals were referenced to crank angle degree (CAD) by an AVL 364 encoder with a 0.2 CAD resolution. Injector energizing profiles were also acquired using six injector clamps. A NI PXIe 1071 acquisition board was used to acquire the high frequency signals. The high reactivity and low reactivity fuel consumption was measured in a mass basis by means of two AVL 733 S balances, while the air mass flow was obtained by means of an Elster RVG G100 sensor. The average temperature and pressure values were obtained in different locations of interest such as the intake and exhaust manifolds and in the high pressure and low pressure EGR lines.

A five-gas Horiba MEXA-7100 DEGR analyzer was used to quantify the pollutants concentration at the exhaust. The gas analyzer configuration allowed to assess the HC, CO, O_2, CO_2 and NOx concentrations. In addition, this gas analyzer is equipped with an additional CO_2 probe to be used in the intake manifold, allowing the instantaneous monitoring of the EGR concentration that was done during the tests. Finally, an AVL 415S smoke meter was used to evaluate the soot emissions produced in each operating condition. The values were reported in filter smoke number (FSN) and then converted to specific soot emissions using the correlation proposed by Northrop et al. [39].

The main modifications in the originally CDC ICE consist of reducing the compression ratio from 17.5:1 to 12.75:1 by means of the pistons machining. The new piston bowl geometry was optimized considering the previous results presented by Benajes et al. [40] aiming at low specific fuel consumption ad minimized NOx and soot emissions. Moreover, six port fuel injectors (PFI) where included in the stock manifold to inject the low reactivity fuel (gasoline). Finally, a low pressure exhaust gas recirculation (EGR) system was designed to deal with the requirements of charge dilution that were identified in previous studies [41]. Table 1 summarizes the main characteristics of both stock CDC and modified dual-fuel engine.

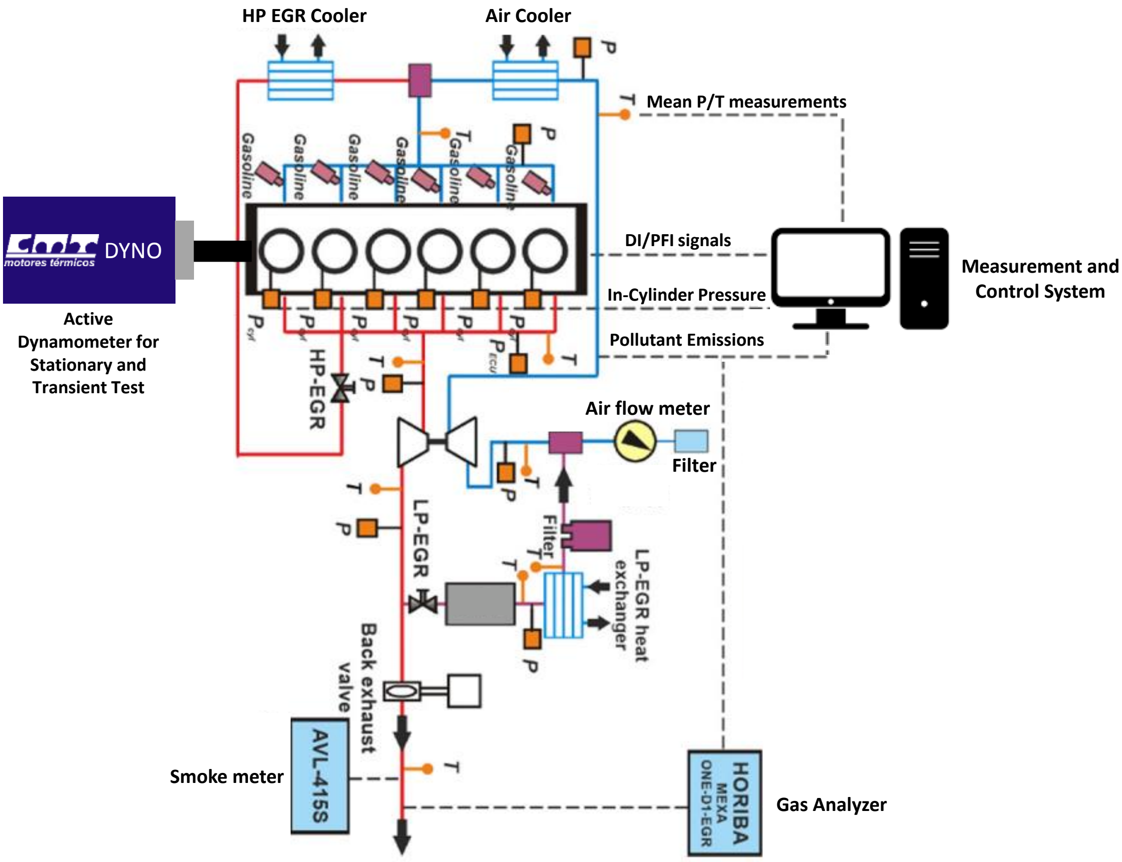

Figure 2 – Experimental test bed facility scheme of the engine and measurement system.

Table 1 – VOLVO MD8K 350 main engine specifications in the commercial original set up and the new RCCI set up.

Parameter	Original Commercial ICE	RCCI ICE
Type	4 stoke, 4 valves	
Nº Cylinders [-]	6	
Displaced Volume [cm^3]	7700	
Stroke [mm]	135	
Bore [mm]	110	
Injection type [-]	DI diesel	DI diesel -PFI gasoline
Compression ratio [-]	17.5	12.8
High pressure EGR [-]	Yes	Yes
Low pressure EGR [-]	No	Yes
Turbo Configuration [-]	VGT	
Rated Power [hp]	$352_{@1800rpm}$	$348_{@1800rpm}$
Rated Torque [Nm]	1453	1444

2.3. Fuel selection for current and future scenarios

Recently, different discussions have been evidenced the role of energy selection on reduction the carbon footprint of vehicles. Figure 3 shows a scheme of different energy solutions that can be used to decarbonize the transportation sector. Despite the claim of lower global efficiency from hydrogen and hydrogen-derived fuels (15%) compared to electrification (75%), it is mandatory to state that the calculations that leads to these values misses fundamental points [42]. Recent studies demonstrated that the use of gaseous and liquid fuels can offer a pathway to transport energy from countries with high potential to renewable power generation, e.g., NEMA region, which yields similar efficiency levels of battery electric vehicles [43]. In this sense, the production paths and utilization routes of hydrogen-based fuels must be understood and explored to enable a global level solution regarding CO_2 reduction rather than local, low efficient and high-cost answer. Figure 3 shows that the combination of highly efficient green electricity production to generate hydrogen and the following reaction with CO_2 from carbon capture techniques offers different fuels, covering a wide range of chemical properties, enabling their use in land, maritime and air transportation. Figure 3 also highlights that bio-fuels and green electricity can be used in combination with other low-carbon fuels to support the decarbonization of the transportation sector. Focusing on the vehicles using internal combustion engines, choosing a suitable fuel for a given combustion concept can be a media to improve the efficiency and reduce the emissions [44]. The use of synthetic (Methanol, e-Fischer-Tropsch, Oxymethylene Dimethyl Ether) and renewable fuels (Bioethanol) provides an edge on carbon dioxide reduction [45][46]. In this sense, different investigation has been made with the engine used in this investigation to determine the most suitable fuels: drop-in fuels (for current scenario) and synthetic fuels (representative of next generation of fuels).

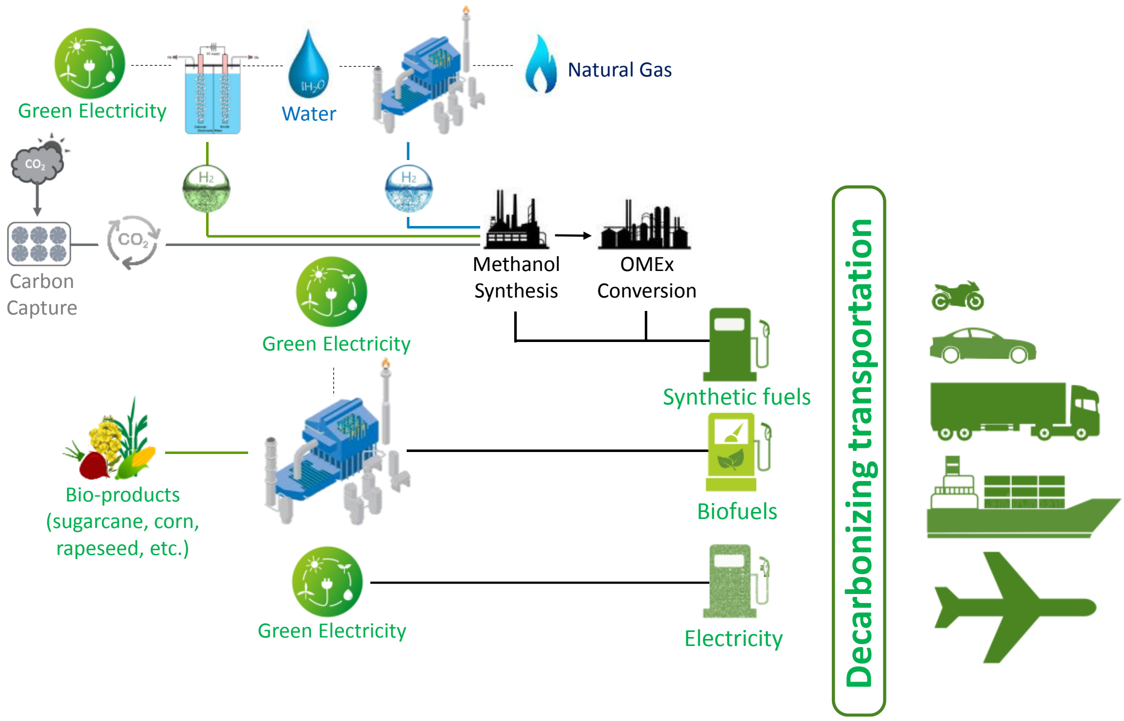

Figure 3 – Low Carbon Fuels production process for transport decarbonization.

For the first case (current scenario), low reactivity fuels with different octane numbers were evaluated, from 80 to 100 [47][48]. The former was assessed as representative of high naphtha content gasoline, which has a much lower well-to-tank CO_2 emissions [49]. The last, RON 100, was investigated as an attempt to improve the combustion process by means of reducing the pressure gradients. As reported in previous works, none of them were able to improve the values of commercial gasoline. It is worth to state that their utilization might be improved if dedicated fuel injection and combustion system were designed for these specific fuels.

Since no benefits were achieved by modifying the low reactivity fuel characteristics, high reactivity fuels that could provide benefits in terms of soot and CO_2 reduction at the same time were investigated. Among the different potential fuels that can be identified in the literature, e-Fischer-Tropsch (e-FT) and Oxymethylene Dimethyl Ether were selected to be assessed due to their similarities with respect to conventional diesel [41]. While e-FT provided significant well-to-wheel CO_2 emissions reduction , their benefits in terms of fuel consumption and emissions (soot and NOx) were limited. The high dilution level, low in-cylinder temperatures and locally rich mixtures have promoted a similar level of emissions than that from the conventional diesel combustion. By contrast, the use of OMEx as HRF enabled the mitigation of soot formation due to its high oxygen concentration in the molecule. At the same time, the use of OMEx allowed to increase the dilution levels, promoting a full engine map with a EUVI NOx compliant calibration at engine-out levels while providing benefits in CO_2 emissions in a WTW basis. Due to the potential presented by this fuel, a complete engine map calibration was performed using commercial gasoline as LRF (see Appendix A, Figure A1). This calibration was selected to be used in this investigation, since it is representative of the best scenario in terms of efficiency and emissions that can be achieved with the DMDF combustion concept.

The TTW CO_2 (tailpipe) is calculated using the CO_2 formation factor (see Table 2). This means a complete combustion after the ATS. The emission results presented in the manuscript are without the ATS (engine-out) except for the CO_2. It is important to note that during experimental test to consider the backpressure of the ATS a valve is calibrated to simulate this effect. For the WTW CO_2 calculation, an in-house life cycle analysis (LCA) model was built. More information about the methodology can be found in [50]. It is important to remark that in the case of OMEx the average between blue (from natural gas with CO_2 capture) and green (from wind and solar power) OMEx production was taken thinking in a future scenario where several production pathways will be required for the large-scale application as shows Figure 3. Table 2 shows the main properties of the fuels used along the work.

Table 2 – Main fuel properties

Property	Diesel	OMEx	Gasoline
Fuel use [-]	HRF	HRF	LRF
Density [kg/m^3]	838	1067	720
Viscosity [mm^2/s]	2.67	1.18	0.55
Cetane Number [-]	54.0	72.9	-
RON [-]	-	-	95.6
MON [-]	-	-	85.7
LHV [MJ/kg]	42.61	19.04	42.40
Carbon Content [$\%_{mass}$]	85.9	43.6	84.2
Hydrogen Content [$\%_{mass}$]	13.3	8.8	15.8
Oxygen Content [$\%_{mass}$]	0.8	47.1	0
Nitrogen Content [$\%_{mass}$]	0	0.5	0
CO_2 formation [gCO_2/ MJ_{Fuel}]	74.4	84.0	72.9
CO_2 WTT [gCO_2/MJ_{Fuel}]	18.6	-66.4	17.2

2.4. Testing methodology

The methodology proposed for this work is a hardware-in-the-loop testing. First, the engine is calibrated in steady-state conditions with conventional fuels (diesel and gasoline). Then, the complete vehicle is studied by means of a 0-D vehicle model. The powertrain is optimized to achieve EUVI engine-out NOx and soot emissions while minimizing TTW CO_2 emissions. Later, the engine is tested in transient conditions (homologation and real driving cycles showed in Appendix B) in the experimental test bench. Lastly, the process is repeated with OMEx as synthetic fuel. A scheme of the proposed methodology is shown in Figure 4.

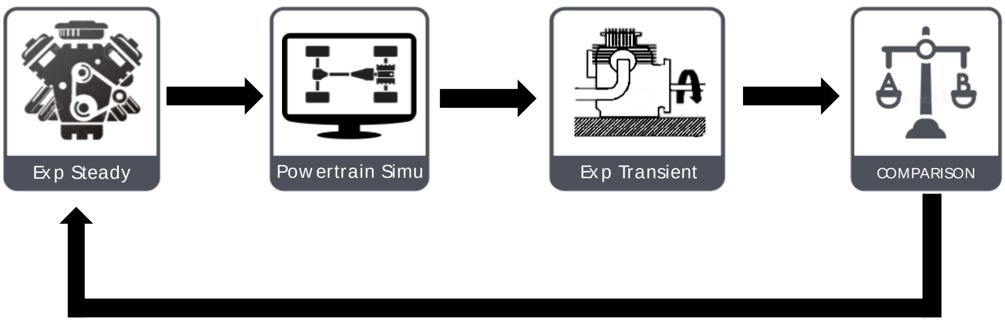

Figure 4 – Testing methodology scheme with the use of conventional and synthetic fuels.

The stationary calibration is performed in order to achieve the best brake thermal efficiency while achieving EUVI NOx and soot at engine-out conditions. The complete calibration maps are those from [11] and are presented in Appendix A. It is important to remark that for the diesel-gasoline calibration it was possible to achieve EUVI engine-out NOx and soot up to 210 hp, 60% of engine load (210 hp). In the case of OMEx-gasoline, the NOx and soot EUVI limits are achieved in the all engine map (up to 350 hp). However, as the generator is designed with a maximum power of 210 hp, the ICE is also used in the mentioned range.

Later, the numerical 0-D vehicle model is run with the experimental data acquired before to reproduce the engine behavior in a map-based approach. The series hybrid powertrain is modeled with the sub-models previously explained. A rule-based controller strategy is used by setting three levels of power (Figure 5). The three level is decided based in previous study of the research group where is seen that higher amount of levels not have any powertrain efficiency improvements and increase the engine transient behavior [42]. A first level was selected at medium engine load (75 hp) in an engine speed with low TTW CO_2 (1500 rpm). The second level represents the best operating condition in terms of TTW CO_2. For both maps, Figure 5 shows that 140 hp at 1500 rpm is the optimum operating condition. An advantage of this selection is that it dispenses the modification of engine speed between the first two levels. Lastly, the third condition is placed at 1800 rpm and 210 hp, representing the maximum power output of the ICE. The change between power levels is done depending on the battery state of charge (SOC). The three levels are symmetrically separated by a parameter called SOC width. When the actual SOC achieves the first SOC charge level, the first power level is applied. If the SOC recovers the initial SOC, the ICE is then turned-off. In case that the SOC continue decreasing, the second level of power is activated. The same approach is applied for the third power level that coincides with the maximum power that the ICE can deliver. It is important to note that for the battery safety, the SOC needs to be maintained between 0.3 and 0.9.

The last parameter optimized is the differential ratio, which influences the traction motor rotational speed and torque. A DoE with several control and component variations was done to obtain the optimum powertrain configuration. For the brevity of the manuscript the detailed optimization for the diesel-gasoline is added in Appendix C. The optimum battery size was 46 kWh, SOC width 2.9% and differential ratio of 9.5:1. This battery size is 8.7 times lower than a pure electric truck (400 kWh) with 300 km of autonomy [51] and 2.0 times lower than a plug-in hybrid (90 kWh) with 60 km of autonomy [52]. In spite of battery size of 20 kWh have close gains to the current selection (Figure C1), in this work the battery size is selected to maximize CO_2 benefits without taking in consideration battery cost.

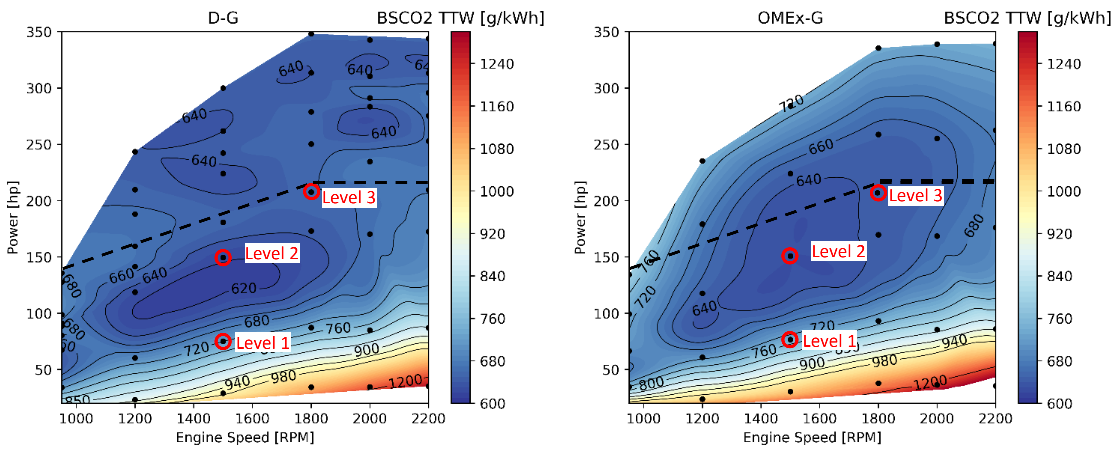

(a) (b)

Figure 5- Operational conditions marked in red over the calibration map for tank-to-wheel (tailpipe) CO_2 with RCCI diesel-gasoline (a) and OMEx-gasoline (b).

To understand the simulation accuracy and possible deviation with respect to a real application, the engine speed and torque profiles are obtained and tested in the engine test bench (transient mode). To broaden the field of study, the homologation cycle with three payloads (0%, 50% and 100%) is tested in the experimental test bench (Figure 6) to compare against the numerical results. Figure 6 shows that only two of the three possible ICE operating conditions are used. Therefore, for the studied cases, the ICE speed is maintained at 1500 rpm when the engine is on, and the load changes. The main difference between cases is the ICE on/off time and the total used time of the ICE. The transient evaluation was performed by an open-loop calibration maps obtained in previous investigations were loaded in the LabVIEW routine [24]. Therefore, the values of VGT position, injection pressure, injection timings, EGR concentration, etc., were obtained from interpolating the open loop maps, like the approach that is used in conventional electronic controller units (ECU). In this case, the engine load demand was provided to the PUMA as time-dependent signal, together with the engine speed from Figure 6. Therefore, the dynamometer could replicate the transient conditions that were defined by means of numerical optimization.

After the transient validation in the experimental test bench, the OMEx-gasoline series hybrid concept is optimized with the same DoE methodology as the diesel-gasoline case. Lastly, the vehicle is simulated in different transient conditions (four driving cycles, see Appendix B, Figure B1, and three payloads, 0%, 50% and 100%) representative of homologation and real driving cycles.

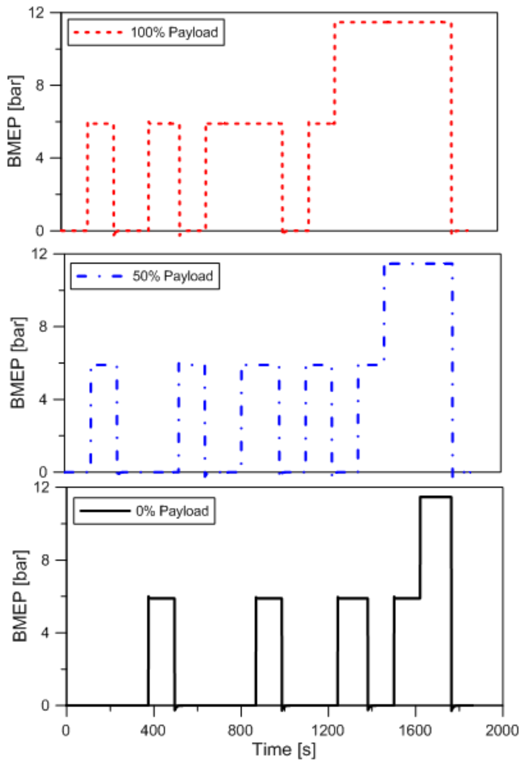

Figure 6- Series hybrid optimum ICE load requirements at 0%, 50% and 100% payload in the WHVC under diesel-gasoline RCCI series hybrid. The engine speed is 1500 rpm when the engine is on.

3. Results and discussion

The results are divided into three subsections. The first one shows the experimental against the simulated ICE behavior in an optimized series hybrid powertrain for WHVC 50% payload using Diesel and Gasoline. The results are also presented for empty and full truck operation. The second subsection shows the powertrain optimization for OMEx synthetic fuel operation under dual fuel combustion. Lastly, the third subsection shows a comparison in 12 operative conditions for both diesel-gasoline and OMEx-gasoline calibration, including TTW and WTW CO_2 results.

3.1. Experimental transient evaluation of the series hybrid RCCI truck concept

The high EGR requirements, the dependence with the inlet temperature, etc., are factors that may hinder the transient application of the RCCI combustion. In this sense, an experimental investigation was performed aiming at quantifying the transient response of the engine compared to the simulation presented in the previous section. This investigation was done at different truck payloads, considering the WHVC driving cycle. For sake of brevity, only the transient results of 50% of payload are presented. Nonetheless, a final table at the end of this section will summarize the results for each one of the payloads investigated. The requirements of engine speed and torque from the simulations can be observed in Figure 7a and Figure 7b. They were used as inputs for the open loop calibration which delivered the air management (Figure 7c, Figure 7d, Figure 7e and Figure 7f) and injections settings (Figure 7g and Figure 7h) of the engine. As it is shown, the experimental profiles follow closely the curves from the simulation. Small variations were attained in the brake torque, but not exceeding 5%, independently on the time. Both experimental intake pressure and air mass flows also exceeded those from the simulations, mainly at 50% of engine load. This might be a consequence of high engine torques. However, low intake temperatures may also increase the air density, enhancing the air management efficiency. It is interesting to note that the open loop calibration approach was able to provide accurate quantities of EGR levels as well as HRF and LRF mass. The former, however, presents a delay, which can be attributed to the long route of the EGR (LP EGR), the valve response and the high gradient which is aimed (from 0% to ≈40%).

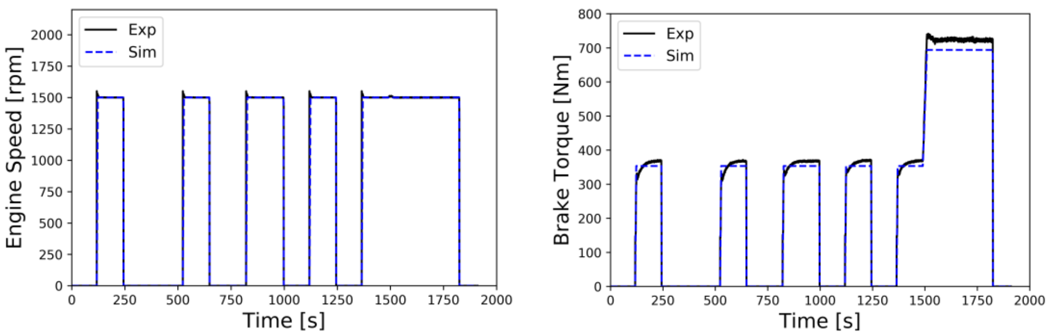

(a) (b)

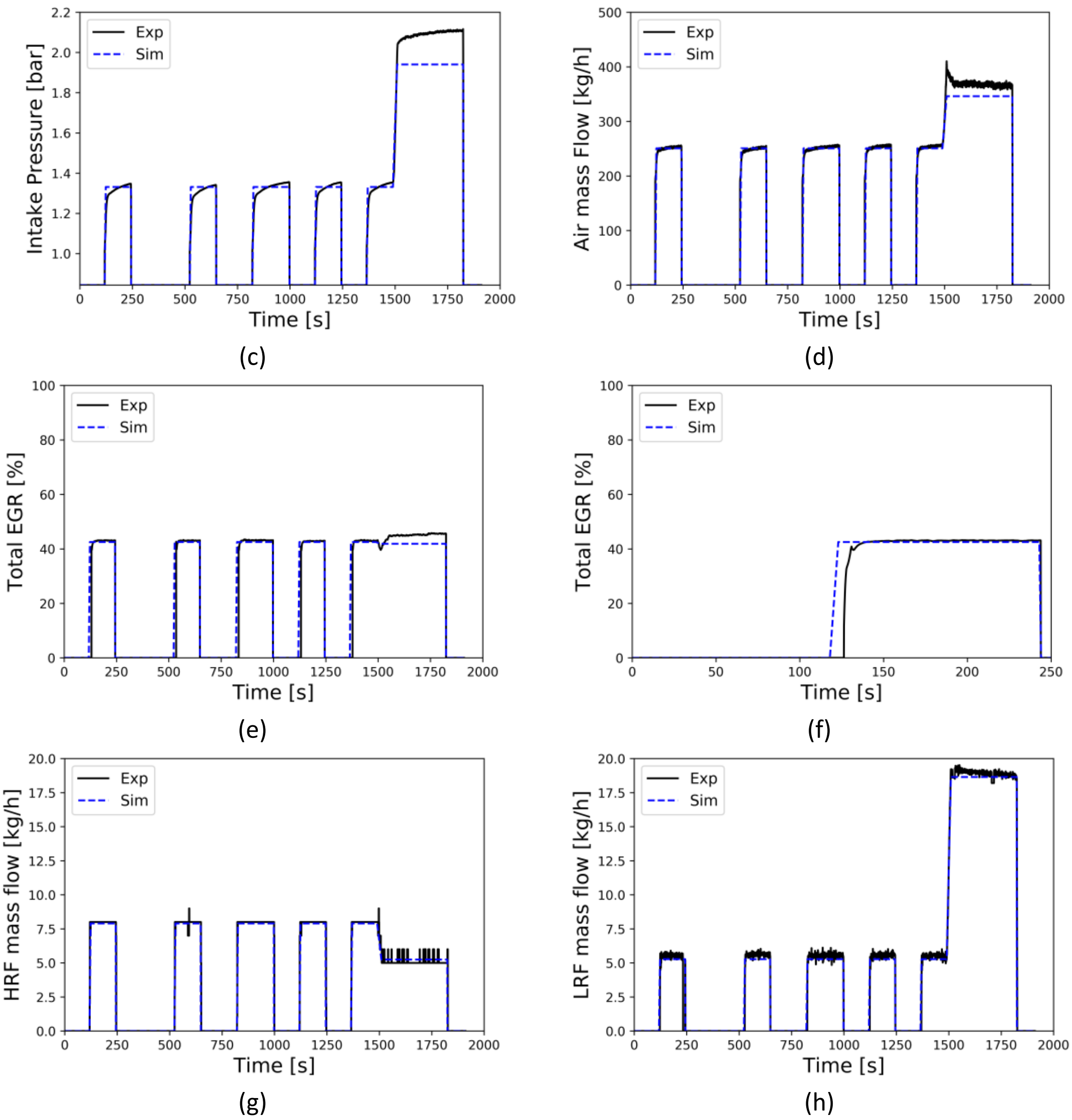

Figure 7- Experimental ICE test bed versus simulated ICE 0D vehicle model results in terms of air management system. WHVC with 50% payload series hybrid RCCI.

A detailed analysis of the temperature response at different locations was performed aiming at quantifying the effect of the start-stops in devices such as compressor, turbine as well as in the EGR, water and oil temperatures (see Figure 8). Overall, all the monitored temperatures presented lower values than the map-based simulation. This is a consequence of the calibration methodology that was used to obtain the steady-state maps, which relied in measuring the operating conditions only with warm engine. Since the transient steps do not include any previous engine warming up, it is expected to have lower temperatures. It is interesting to note that the compressor inlet temperatures are nearly constant during the tests due to low flow of low pressure EGR. As the engine load is increased, higher temperatures are obtained due to the higher energy demand on the heat transfer system of the low pressure EGR. Despite the almost constant temperature at the compressor inlet, compressor outlet temperature is dependent on time, increasing during the period at which the engine is on because of the heat generated by friction and gas compression. The remaining temperatures also follow the same trend as the one verified in the compressor outlet.

In addition, Figure 8 presents the values of turbine inlet, which is a useful metric to quantify the energy available at the exhaust to generate dynamic pressure and also if the combustion process is converging to a steady state operation. As it can be observed, the exhaust temperature does not achieve steady-state operation in none of the steps of the engine. This can be correlated with the fact that the engine never attains its thermal stability as it can be inferred from the results of water and oil temperatures. Finally, the HP EGR inlet temperature also follows the trend of the turbine inlet temperature, since it is derived before the turbine.

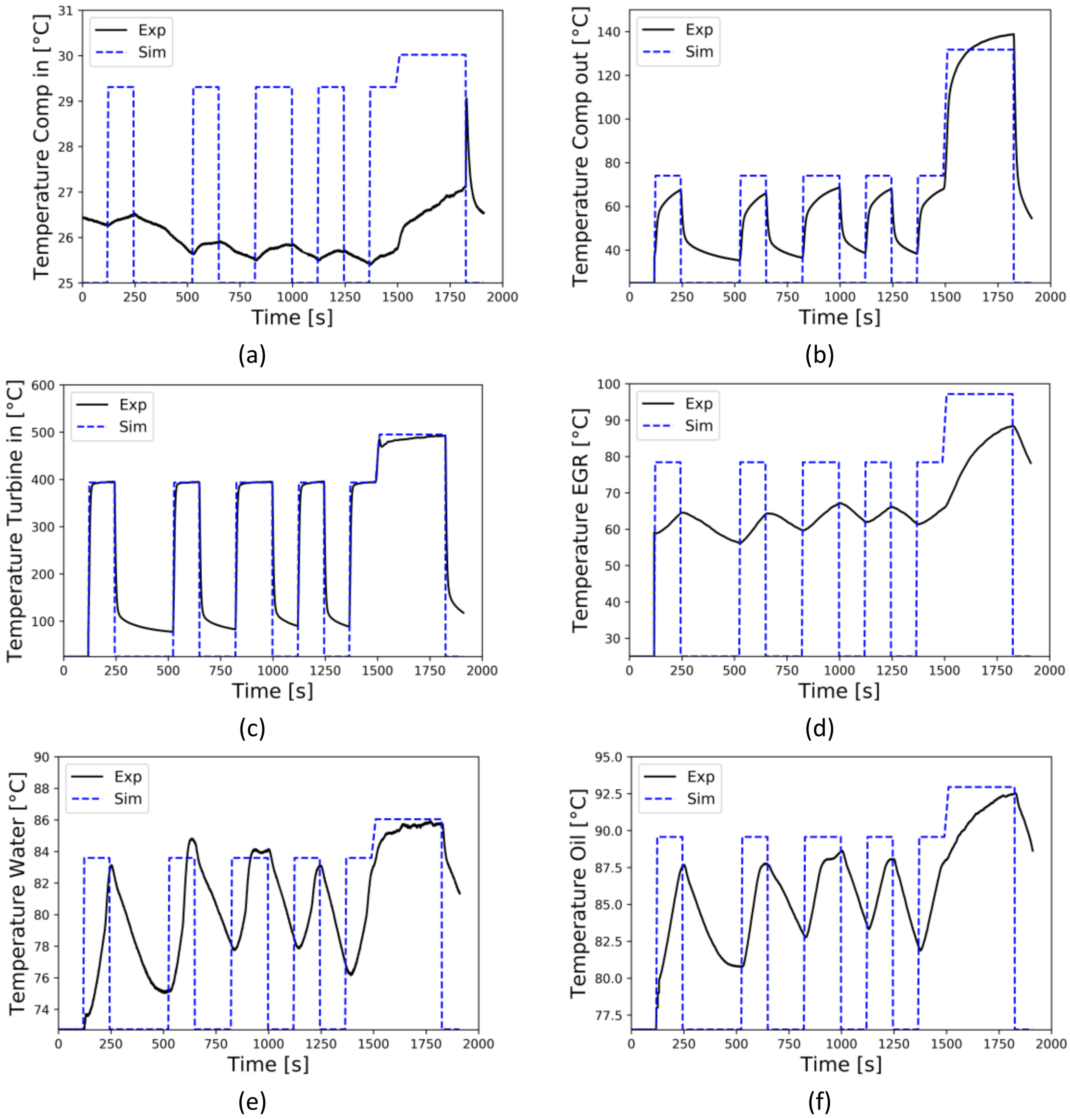

Figure 8- Experimental ICE test bed versus simulated ICE 0D vehicle model results in terms of ICE temperatures. WHVC with 50% payload series hybrid RCCI.

The transient in the temperature values has direct effects on the combustion development. This can be observed in Figure 9, where different metrics such as combustion phasing, end of combustion, maximum in-cylinder pressure and pressure gradient are provided. The lower temperatures at the beginning of the steps leads to reductions in the in-cylinder reactivity, which enlarge the ignition delays, shifting the combustion process towards the expansion stroke. Both Figure 9aand Figure 9b demonstrates this effect, confirming delayed combustion phases and end of combustion for the early stages of the steps. As the time proceeds, the engine starts to warm and the combustion is progressively advanced due to the high temperatures in the intake manifold as presented in Figure 8b, approaching to the values obtained in the steady-state calibration. This slow response of the combustion process may be the reason for the difficulties in obtaining the torque demand in the early stages of the step. Advanced control techniques such as the one used by Guardiola et al. [53] offer a solution to tailor the engine settings, avoiding this slow combustion response.

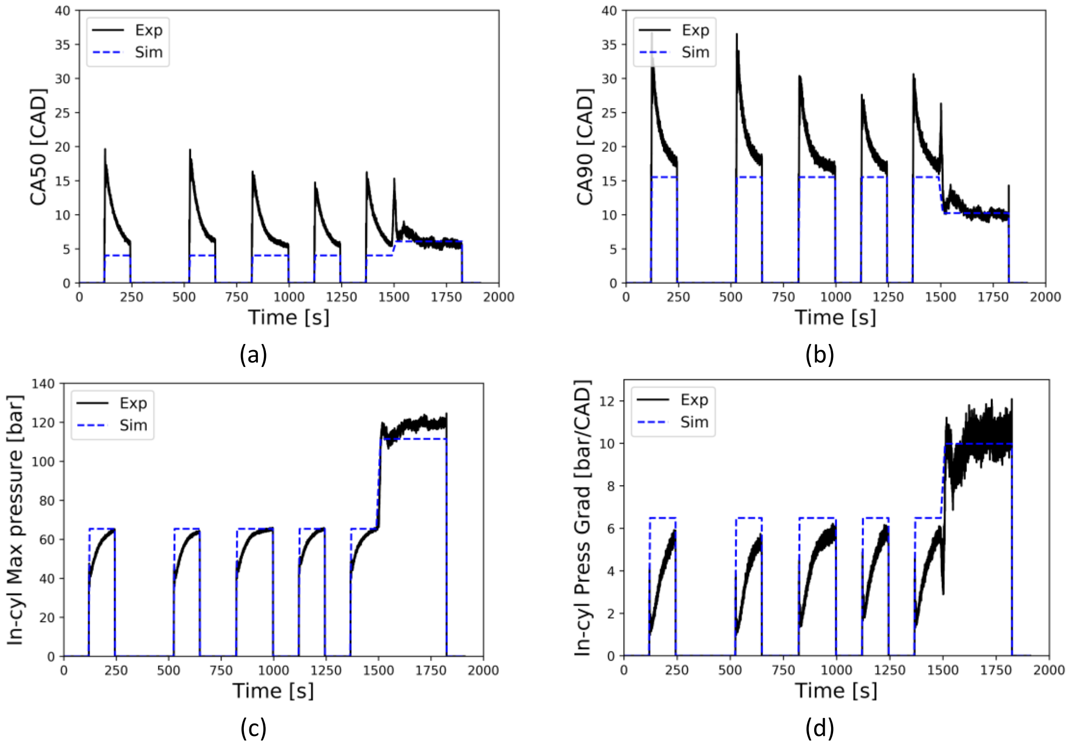

Figure 9- Experimental ICE test bed versus simulated ICE 0D vehicle model results in terms of combustion parameters. WHVC with 50% payload series hybrid RCCI.

The differences in the combustion development between the simulated and experimental results may affect the emissions production during the cycle. Emissions as NOx and uHC are highly dependent on the combustion chamber temperature. This can be confirmed by analyzing Figure 10, where the evolution of the instantaneous NOx emissions during the transient cycle is presented. As it can be observed, there is a direct correlation between the cases with delayed combustion process and the zones with low NOx production. Most of the experimental results for this pollutant under predicts the values of the steady-state calibration. Despite of not being an apparent issue from an emission regulation perspective, these low NOx levels may indicate losses in thermodynamic efficiency, which is a consequence of the delayed combustion process as demonstrated in Figure 9. Nonetheless, from the analysis of the CO_2 instantaneous profiles (Figure 10), it can be inferred that, if the efficiency losses exist, they are not high enough to provide divergences between the experimental and simulated CO_2 profiles [54].

The modifications of the combustion process also impact the production of both

CO and HC emissions in different manners as it is shown in Figure 10c and Figure 10d, respectively. This is a consequence of the different mechanisms that are responsible for each emission formation [54]. In the RCCI combustion, CO emissions are mainly produced in rich zones, where there is not enough oxygen to oxidize the CO to CO_2. Lower temperatures may reduce the reaction rates of the oxidation paths, but this mechanism does not seem to be affected in this case, since the CO emission are like those of the simulation cases. On the other hand, HC emissions are significantly increased compared to the simulated cases. This effect can be attributed to the HC formation mechanism in RCCI combustion. Since a high quantity of fuel is injected by means of port fuel injection, it tends to be directed towards the piston crevices during the compression stroke, where it cannot be burnt due to the high heat losses near to the cylinder wall. The low cylinder block temperatures enhance the heat loss process, hindering the fuel oxidation. This effect starts to be reduced as the cycle approaches to the final phase, where the engine is close to warm conditions. At this period, the instantaneous HC production is like that obtained with the steady-state calibration.

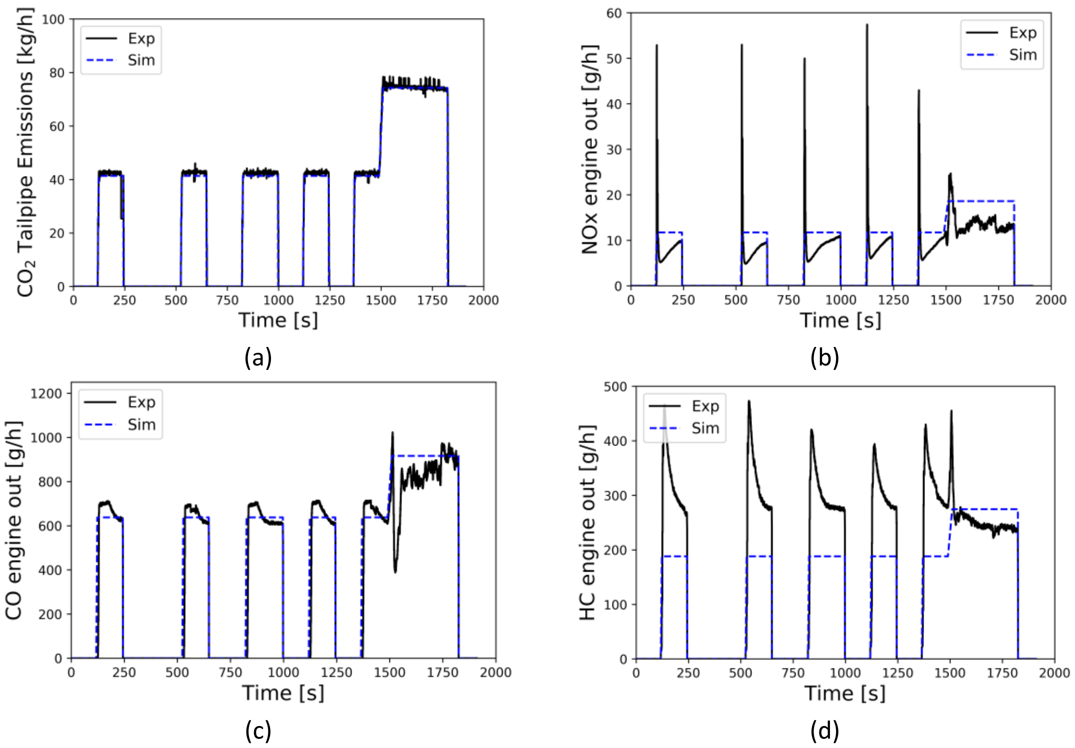

Figure 10- Experimental ICE test bed versus simulated ICE 0D vehicle model results in terms of instantaneous emissions. WHVC with 50% payload series hybrid RCCI.

The instantaneous results from fuel consumption and emissions were integrated with respect to time to deliver the evolution of the cumulative profiles, allowing to quantify the differences at the end of the transient cycle (see Figure 11). Fuel consumption results have demonstrated high similarity between the experimental and simulated values, which can be attributed to the similar consumption of low and high reactivity fuels. By contrast, emissions have demonstrated higher deviation due to the influence of the wall temperature and the combustion process in their formation compared with the steady-state conditions. NOx emissions presented a total deviation of 24% at the end of cycle, which is attributed to the general delayed combustion process Figure 9. The differences are steeply increased during the cycle, as it can be observed in Figure 11c and Figure 11d. for CO and HC emissions, were also negatively impacted. The former presents the major differences at the end of the cycle because of the difference for the operating condition with 50% of engine load. Nonetheless, the differences were around 7% considering the final cumulative results. HC emissions have the opposite trend than NOx with an underestimation of the numerical calculation totalizing more than 23% of difference.

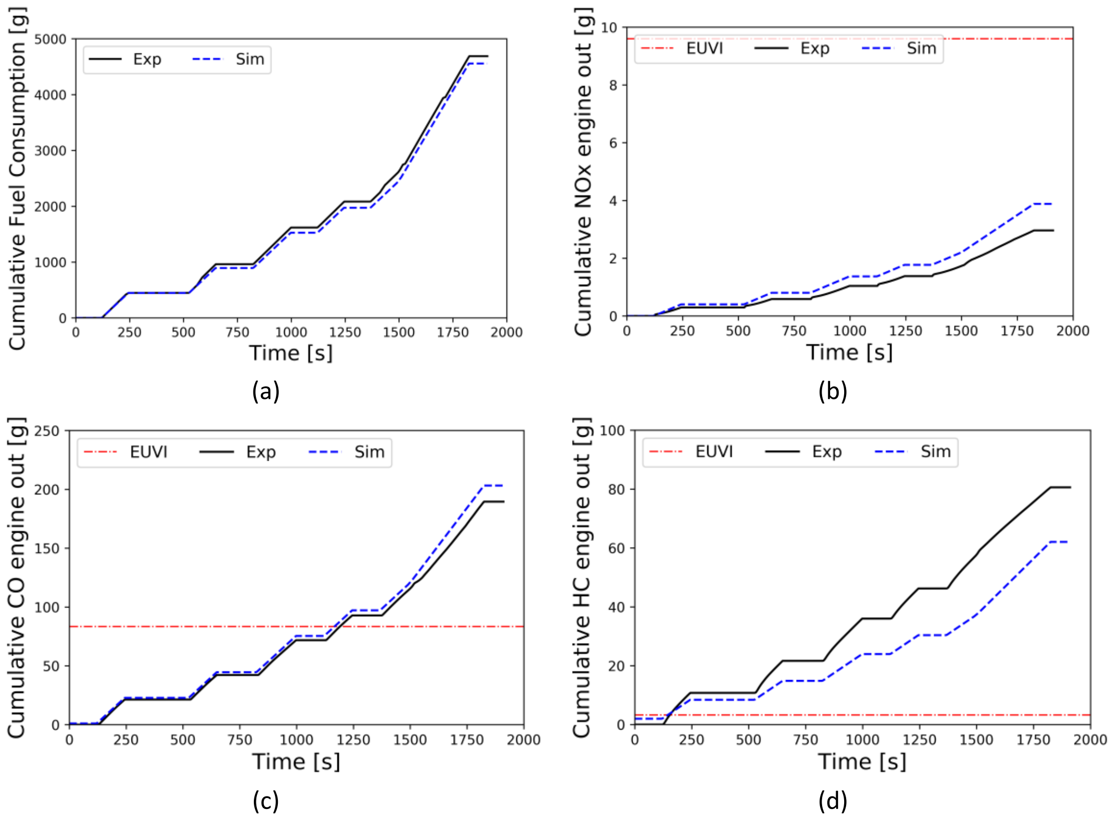

Figure 11- Experimental ICE test bed versus simulated ICE 0D vehicle model results in terms of cumulative emissions. WHVC with 50% payload series hybrid RCCI.

The same simulation methodology was applied for the remaining payloads in the case of RCCI D-G, enabling to compare the differences between the simulation and the real driving conditions for a wide set of operating conditions. The results are presented in Table 3. It is possible to see that the increase in payload reduces the fuel consumption and emissions differences. The closest results are the fuel consumption (equivalent to the tailpipe CO_2 emissions) with a maximum difference of 3.6% at empty truck. The simulation always under predicts the experimental measurement. This behavior is attributed to the lower engine temperatures, increasing the required fuel to achieve a similar brake torque. In terms of pollutant emissions, the NOx and CO are over predicted meanwhile the HC levels are under predicted. As it was seen in Figure 8 and Figure 9, the lower engine temperatures change the combustion parameters and combustion chamber temperatures. The NOx strongly decreases the prediction differences between 30% to 3% due to higher engine use requirements, increasing with the overall cycle operation temperature. The HC emissions present similar behavior, but only achieve a minimum of 10% at full payload. The CO show the most stable measurement with differences around 5.5% for all payloads in average.

Table 3 – Comparison experimental ICE test bed versus simulated ICE 0D vehicle model results in terms of cumulative fuel consumption and emissions in grams and percentage differences. Case WHVC with 0%, 50% and 100% payload series hybrid RCCI.

Payload	**Fuel [g]**			**NOx [g]**			**HC [g]**			**CO [g]**		
	Exp	Sim	Diff	Exp	Sim	Diff	Exp	Sim	Diff	Exp	Sim	Diff
0%	3000	2892	-3.6%	1.74	2.50	+30%	59.5	41.0	-31%	123	132	+7%
50%	4704	4557	-3.1%	2.97	3.88	+24%	80.5	62.1	-23%	190	203	+7%
100%	6373	6284	-1.4%	5.11	5.29	+3%	92.7	83.1	-10%	244	254	+4%

Figure 12 shows the Kernel Density Estimation (KDE) plots for some of the relevant temperatures of engine operation. More specifically, the engine oil and water temperature are presented as an indicative of the engine warm up while the EGR temperature was selected to represent the influence on the combustion outcomes evolution (since it is dependent on the exhaust gas temperature). The assessment was performed for the three different payloads. The water and oil temperature show that the increase in the truck cargo mass has a positive effect in the engine conditions with a major concentration of points in the high temperatures for 100% than 0%. This allows to conclude that the use of high payloads leads to shorter transients in engine operation, benefiting the steady-state operation and the emission control. Despite the differences observed in water and oil temperatures, the major discrepancies are seen in the air management system. Figure 12c shows the experimental EGR temperature distribution in the different payloads while Figure 12d depicts the differences between the experimental results and those obtained from the steady state simulation. It is interesting to note that the temperature distribution does not follow a linear dependence with respect to the payload. As it can be observed, a small variation is obtained from the 0% to 50 % of engine payload, compared to the 50% to 100% of payload. This last step shows that the temperature evolution is enhanced towards high temperature values. This concurs with the results present for the transient NOx profiles, which depicted a fast evolution of NOx emissions towards the steady state condition for the case with 100% of payload. Therefore, it can be concluded that once the engine approaches to warm operation, closer are the results compared to the simulation, re-affirming the results seen in Table 3.

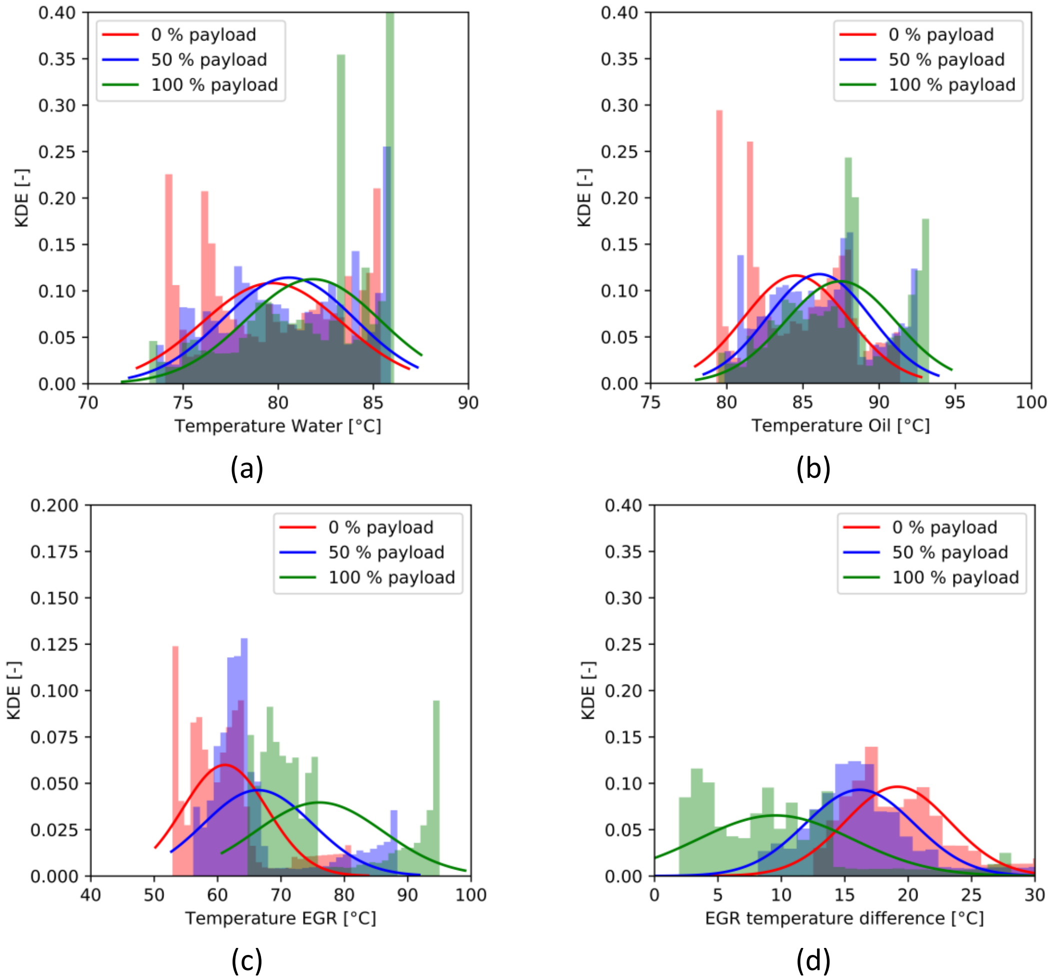

Figure 12- Kernel density estimation distribution of experimental engine water (a), experimental engine oil (b), experimental EGR (c) and difference between experimental and simulated EGR (d) temperatures.

Table 4 shows the same results than Table 3 but in brake specific basis. This allows to understand the mean fuel consumption of the concept and if it is possible to achieve the EUVI legislation for the different pollutant emissions. The fuel measurements and simulations show that the values decreased with the payload with a minimum of 217 g/kWh of fuel consumption at full payload. In terms of emissions, NOx is far below the EUVI (0.46 g/kWh) and close to the CLOVE scenario A for EUVII (0.12 g/kWh) without the requirements of any ATS [55]. The HC and CO are far from EUVI (0.16 g/kWh and 4.0 g/kWh, respectively) [56]. In a no-hybrid case, the authors show that the OEM DOC can deal with the amount of HC and CO at medium and high payloads [57].

Table 4 – Comparison experimental ICE test bed versus simulated ICE 0D vehicle model results in terms of cumulative fuel consumption and emissions in grams per kWh. Case WHVC with 0%, 50% and 100% payload series hybrid RCCI.

Payload	Fuel [g/kWh]		NOx [g/kWh]		HC [g/kWh]		CO [g/kWh]	
	Exp	Simu	Exp	Simu	Exp	Simu	Exp	Simu
0%	232	223	0.13	0.19	4.60	3.17	9.5	10.2
50%	226	218	0.14	0.19	3.86	2.98	9.1	9.7
100%	217	214	0.17	0.18	3.15	2.83	8.3	8.7

3.2. Synthetic Fuels Powertrain Optimization

A similar approach than that for diesel-gasoline is applied for the OMEx-Gasoline case. The energy management system (SOC width), battery size and differential ratio is optimized using a DoE. Figure 13a show that the battery size selected is close to that of the diesel-gasoline case, with a battery size of 31 kWh instead of 46 kWh. In addition, the differential ratio was also similar, with an optimum of 8.5 for OMEx-G instead of 9.5 for D-G. The SOC width is 1.5% for OMEx-G and 2.9% for the D-G case. It is clear that the best hardware configuration has small changes depending on the fuel used due to the similarities in terms of the engine calibration. Similar operating conditions are used due to the best brake specific fuel consumption at 1500 rpm and medium engine load. This is a strong point for the concept because it allows to change the fuels without changing the powertrain. It will require only to change the engine electronic unit configuration to operate with OMEx instead of diesel. It is important to remark that for OMEx-G the benefits in TTW CO_2 are 2% against the non-hybrid Diesel case. This is 1.3% lower than the D-G hybrid case due to higher tailpipe emissions of the calibration map (see Figure 5).

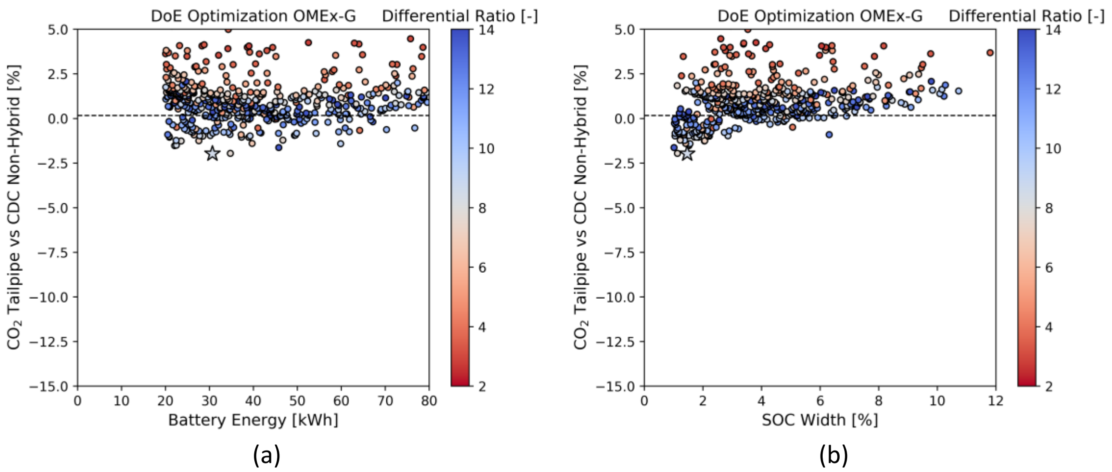

Figure 13 - DoE optimization for OMEx-gasoline in terms of TTW CO_2 reduction for battery size (a) and SOC width (b) in the WHVC at 100% payload. The color bar shows the differential ratio range.

Figure 14 shows the operating points during the driving cycle in the calibration map of TTW and WTW CO_2 emissions for OMEx-gasoline RCCI combustion in the series hybrid powertrain. In spite of that at TTW level the OMEx-G has slightly higher emissions, the WTW CO_2 shows the potential of the synthetic fuel. The values for OMEx-G achieve 700 g/kWh while the D-G case is around 800 g/kWh.

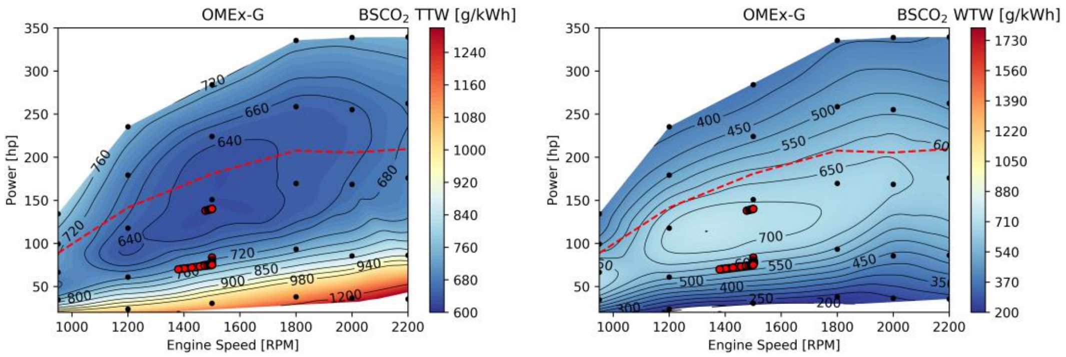

(a) (b)

Figure 14- Engine map operating condition at 50% payload in the WHVC with OMEx/gasoline.

Figure 15 shows the cumulative CO_2 tailpipe emissions and engine-out NOx for the series hybrid case at different payloads. For reference, the non-hybrid CDC case of is added. In the cumulative results it is possible to see the stepped behavior of the series hybrid as well as the reduction in emissions of the proposed concept. The CO_2 benefits strongly increase with the payload due to the low efficiency of the non-hybrid case at low engine loads (low truck cargo mass). In addition, the series hybrid reduces the electric losses thanks to low energy requirements along the driving cycle. The engine-out NOx emissions strongly decrease for the OMEx-gasoline RCCI operation in the series hybrid powertrain. The low temperature in the combustion chamber plus the ICE control in selected points achieves a 90% of NOx reduction with negligible soot emissions.

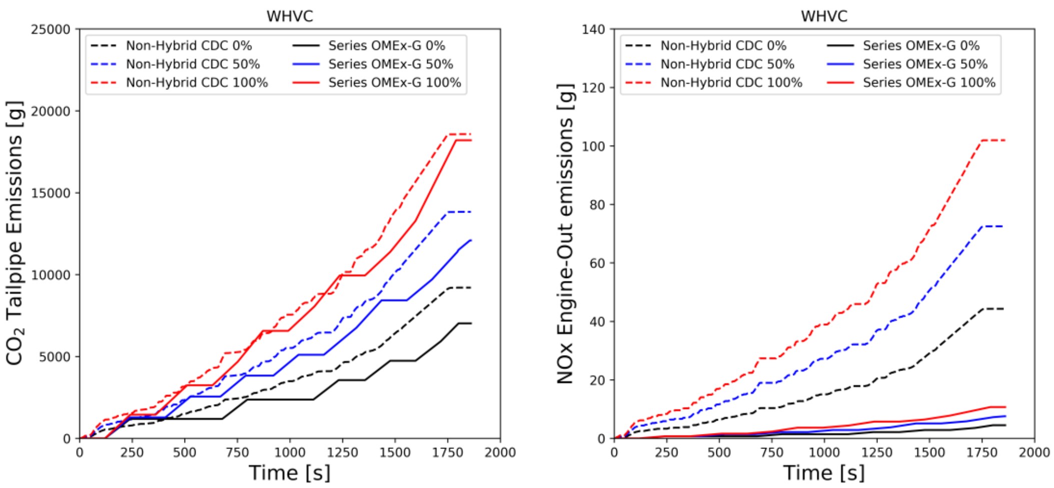

(a) (b)

Figure 15- Engine map operating condition at 50% payload in the WHVC with OMEx/gasoline.

3.3. Synthetic Fuels vs Conventional Fuels in Transient conditions

The optimum cases for both RCCI cases are tested in different driving cycles and payload conditions. Figure 16 shows the TTW, WTW CO_2 emissions and volumetric fuel consumption differences with respect to the CDC non-hybrid (OEM Truck) case. It is important to note that the balls with red edge implies the achievement of 2030 CO_2 reduction (30%) and black edge the 2025 target (25%). The non-hybrid DMDF cases are also added for comparison. This last case represents the truck with the original powertrain but with the calibration of the ICE changed to operate in the complete engine map to achieve the same power output that the OEM case. Figure 16a show that it is possible to achieve 30% of tailpipe CO_2 reduction in low payload and urban cases for both fuels. The improvements are higher for the diesel-gasoline case than for OMEx-gasoline due to the higher brake thermal efficiency and low carbon-to-fuel conversion ratio. The urban case shows large CO_2 benefits in all the payloads with a maximum of 38% at empty truck and 10% at full payload. The Flat driving cycle, which has the highest average speed and lowest deceleration time and stop time (Table), is the most demanding cycle with only 10% of benefit at empty truck and CO_2 penalization of 6% at full load condition. The average benefits in the 12 conditions tested are 11.5% for diesel-gasoline and 10.0% for OMEx-gasoline. The non-hybrid with both fuels has a penalization of 1% with respect to the OEM truck.

Figure 16b shows the WTW CO_2 differences using the methodology presented in section 2.3. The use of conventional fuels does not have any significant advantage in WTW CO_2 with similar results presented in tailpipe conditions. However, when synthetic fuels are introduced, the benefits are large. In the case of the non-hybrid OMEx-gasoline, the benefits are between 70% (urban low payload) and 30% (flat and high payload). For the series hybrid, the OMEx-gasoline the benefits are 40% to 15%. The higher advantages for the non-hybrid with respect to the series platform are related to the gasoline fraction used. For the non-hybrid case, the gasoline fraction is around 50% due to the use of low load conditions (see Appendix, Figure A1). In the case of the series hybrid, the GF is around 80% due to the three operational points used. This means that the diesel substitution for OMEx has lowest impact than in the case of the non-hybrid powertrain. A conclusion from this analysis is that the search of a low reactivity fuel with similar benefits (brake thermal efficiency and soot emissions) than OMEx is a good alternative for this type of hybrid powertrain.

Despite that the WTW CO_2 emissions are higher for the non-hybrid than for the series hybrid, the volumetric fuel consumption (Figure 16c) shows that the OMEx use implies large volumetric fuel use. The non-hybrid platform consumes 40% more volume in average than the OEM truck. This is due to the low LHV of the OMEx. Therefore, this implies higher fuel tank, more weight to be transported and the OMEx cost needs to be strongly lower than Diesel to be applied. In this sense, the series hybridization allows the OMEx-gasoline concept to consume only 9.8% more fuel volume than the diesel non-hybrid platform. The diesel-gasoline series hybrid case reduces the volumetric fuel consumption 1.6% in average and the of non-hybrid diesel-gasoline case increases it by 6.9% in average. Therefore, the series hybrid allows to maintain the fuel consumption in reasonable values, with a strong decrease of the CO_2 emissions in both TTW and WTW bases.

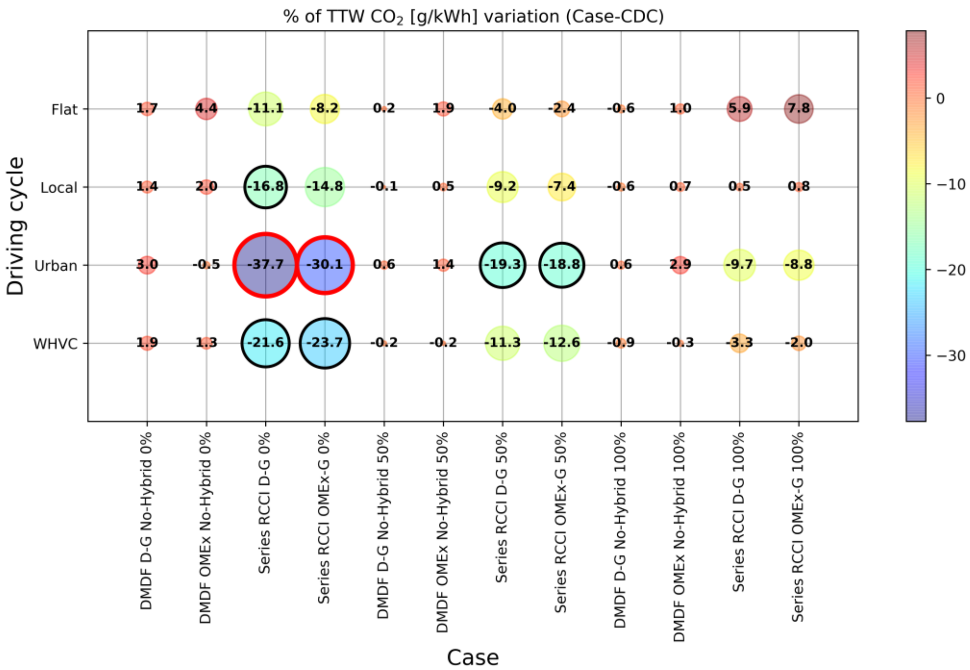
% of TTW CO_2 [g/kWh] variation (Case-CDC)
Driving cycle
Flat
Local
Urban
WHVC
Flat: 1.7 4.4 -11.1 -8.2 0.2 1.9 -4.0 -2.4 -0.6 1.0 5.9 7.8
Local: 1.4 2.0 -16.8 -14.8 -0.1 0.5 -9.2 -7.4 -0.6 0.7 0.5 0.8
Urban: 3.0 -0.5 -37.7 -30.1 0.6 1.4 -19.3 -18.8 0.6 2.9 -9.7 -8.8
WHVC: 1.9 1.3 -21.6 -23.7 -0.2 -0.2 -11.3 -12.6 -0.9 -0.3 -3.3 -2.0
0
−10
−20
−30
DMDF D-G No-Hybrid 0%
DMDF OMEx No-Hybrid 0%
Series RCCI D-G 0%
Series RCCI OMEx-G 0%
DMDF D-G No-Hybrid 50%
DMDF OMEx No-Hybrid 50%
Series RCCI D-G 50%
Series RCCI OMEx-G 50%
DMDF D-G No-Hybrid 100%
DMDF OMEx No-Hybrid 100%
Series RCCI D-G 100%
Series RCCI OMEx-G 100%
Case

(a)

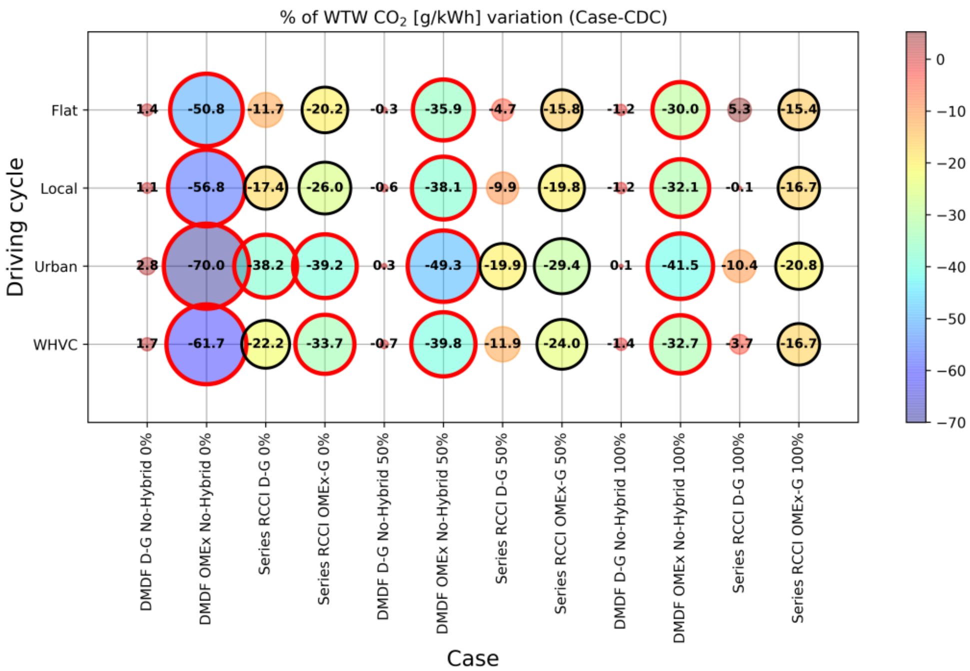
% of WTW CO_2 [g/kWh] variation (Case-CDC)
Driving cycle
Flat
Local
Urban
WHVC
Flat: 1.4 -50.8 -11.7 -20.2 -0.3 -35.9 -4.7 -15.8 -1.2 -30.0 5.3 -15.4
Local: 1.1 -56.8 -17.4 -26.0 -0.6 -38.1 -9.9 -19.8 -1.2 -32.1 -0.1 -16.7
Urban: 2.8 -70.0 -38.2 -39.2 0.3 -49.3 -19.9 -29.4 0.1 -41.5 -10.4 -20.8
WHVC: 1.7 -61.7 -22.2 -33.7 -0.7 -39.8 -11.9 -24.0 -1.4 -32.7 -3.7 -16.7
0
−10
−20
−30
−40
−50
−60
−70
DMDF D-G No-Hybrid 0%
DMDF OMEx No-Hybrid 0%
Series RCCI D-G 0%
Series RCCI OMEx-G 0%
DMDF D-G No-Hybrid 50%
DMDF OMEx No-Hybrid 50%
Series RCCI D-G 50%
Series RCCI OMEx-G 50%
DMDF D-G No-Hybrid 100%
DMDF OMEx No-Hybrid 100%
Series RCCI D-G 100%
Series RCCI OMEx-G 100%
Case

(b)

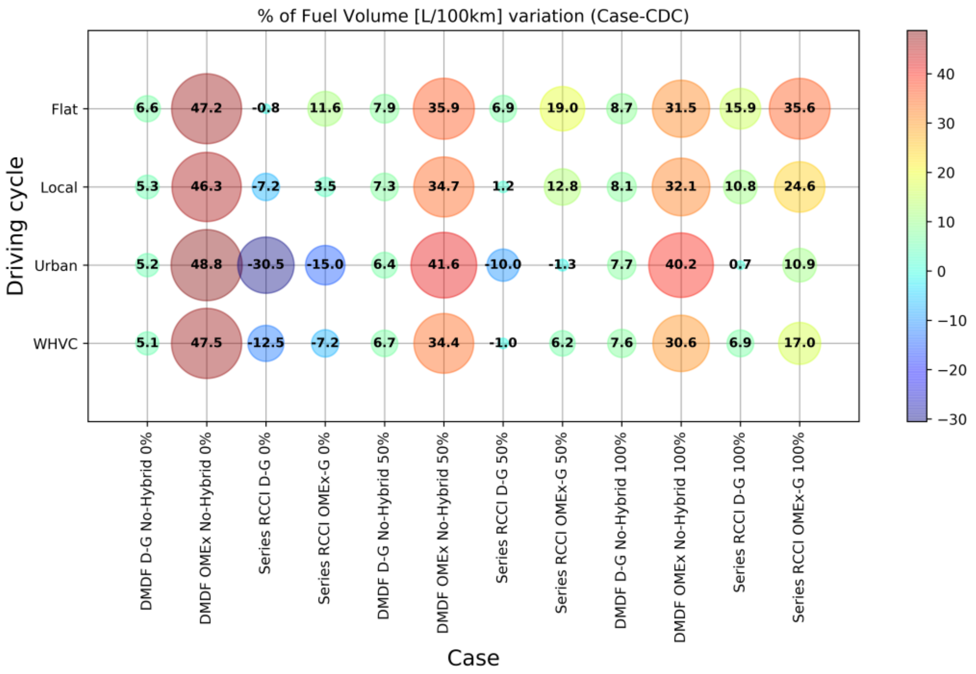

(c)

Figure 16- Tank-to-Wheel CO_2 (a), Well-to-Wheel CO_2 (b) and Volumetric Fuel consumption (c) differences with respect to CDC non-hybrid for four driving cycles and three payload conditions.

Figure 17 shows that NOx and soot emissions are significantly improved by the proposed concept. The Figure 17 shows that NOx is reduced around 90% with all the concepts including the non-hybrid one thanks to the ultra-low NOx calibration. In the case of soot, the reduction is 100% for the OMEx cases with and without hybridization due to the oxygen content in the fuel molecule, which allows the full carbon oxidation and the absence of direct carbon-carbon bonds. In the case of conventional fuels, the ICE de-rating in the series hybrid allows to achieve EUVI at engine-out levels with 92% of soot reduction in average. It is important to note that the circles with black edge implies EUVI limit compliment. These results present a relevant improvement compared to the conventional DMDF calibration since it does not allow to achieve EUVI soot emissions in all conditions. All the cases with 100% payload exceed the EUVI limit as well as 50% payload in the flat driving cycle.

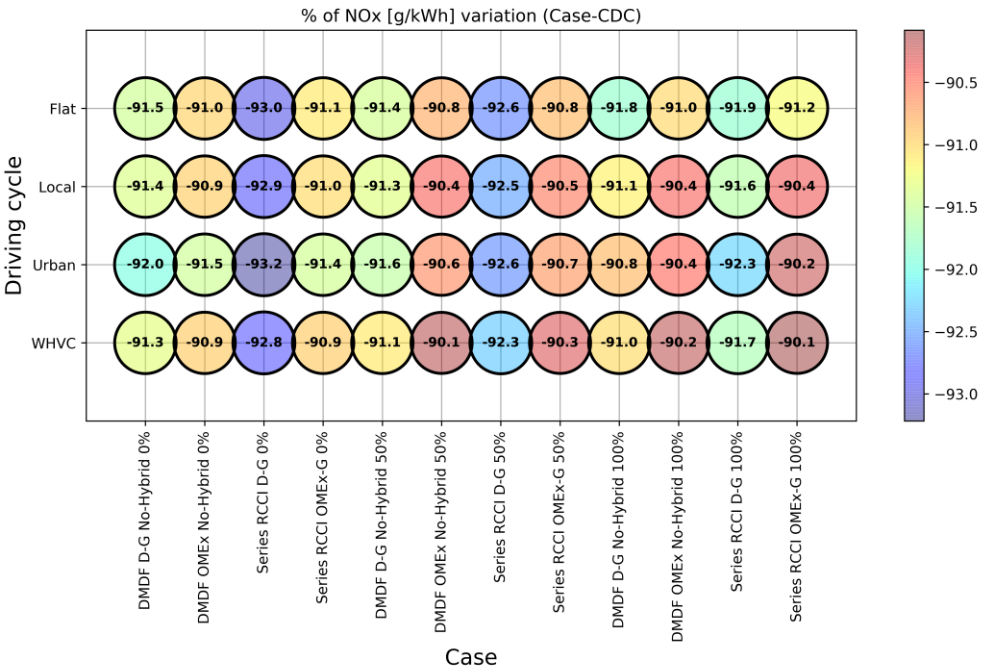

(a)

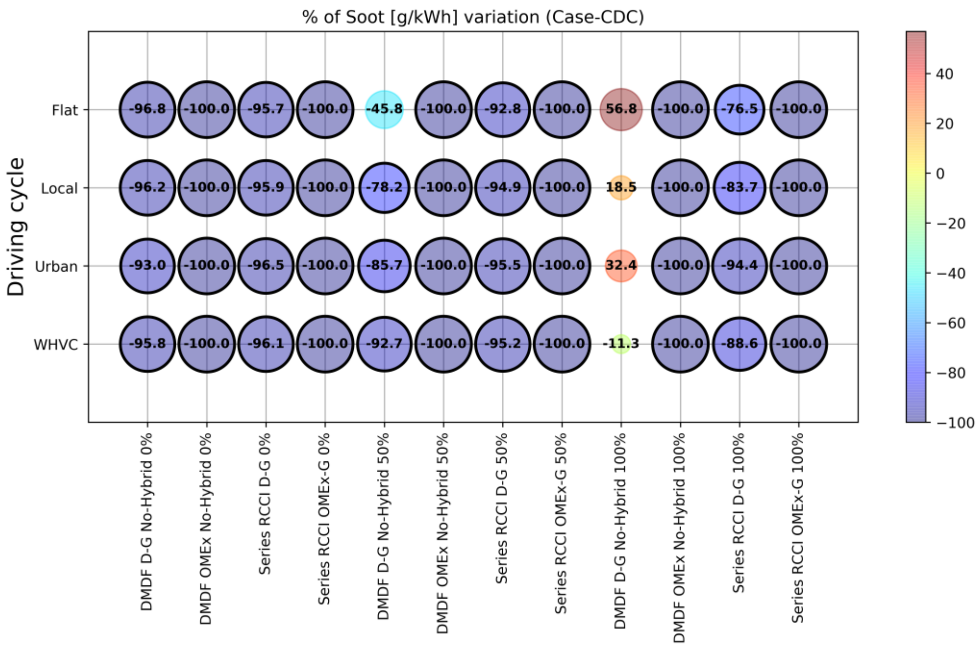

(b)

Figure 17- NOx (a) and soot (b) emissions differences with respect to CDC non-hybrid for four driving cycles and three payload conditions.

4. Conclusions

The manuscript shows the optimization of a dual-fuel series hybrid concept with conventional and synthetic fuels. OMEx is used as high reactivity fuel due to the ultra-low carbon footprint and the possibility to avoid the soot production. In addition, the dual-fuel concept helps to reduce the volumetric fuel consumption thanks to the injection of gasoline. A complete calibration map, followed by a numerical powertrain design and an experimental engine validation under transient conditions was presented. The main findings of this work are:

- The powertrain design shows similar battery requirements 31 kWh for OMEx-G and 46 kWh for D-G with differential ratio of around 9:1 and SOC width control of 2%. At full truck operation the CO_2 tailpipe benefits are 3.3% for D-G and 2.0% for OMEx-G with respect to the OEM CDC truck.
- The experimental evaluation in transient conditions shows fuel consumption deviations between the simulated and experimental values below 3.6%. Therefore, the CO_2 tailpipe prediction using engine map-based method have good precision.
- The pollutant emissions deviation between experimental and simulated suffer a strong impact depending on the truck payload due to the transient combustion chamber temperatures. At empty truck conditions, the NOx is over predicted by 30%, meanwhile at full payload is only 3% over predicted. The CO were close between simulated and experimental with an over prediction of 5% in average. However, the overprediction put in a safe size the simulation results, showing the great potential of RCCI combustion in series hybrid.
- The main problem of the proposed concept is the uHC, due to the excessive amount and the under prediction of the model with variations between 30% and 10%. A separate analysis needs to be done with DOC experiments to find the solution for this point.
- The evaluation under real driving cycles highlighted the potential of the concept in urban areas with tailpipe reductions of 35% with the empty truck and 10% at full payload. The evaluation in WTW CO_2 levels shows large improvements in this cycle with around 40% and 15% with respect to OEM CDC truck.

The CO_2, NOx and soot were strongly reduced with respect to the commercial current application in both dual-fuel concepts. These are positive results for the next generation of more clean trucks.

5. Acknowledgments

The authors thanks ARAMCO Overseas Company and VOLVO Group Trucks Technology for supporting this research. The authors also acknowledge the Conselleria de Innovación, Universidades, Ciencia y Sociedad Digital de la Generalitat Valenciana for partially supporting this research through grant number GV/2020/017. Operación financiada por la Unión Europea a través del Programa Operativo del Fondo Europeo de Desarrollo Regional (FEDER) de la Comunitat Valenciana 2014-2020 con el objetivo de promover el desarrollo tecnológico, la innovación y una investigación de calidad. Proyecto IDIFEDER/2020/34, Equipamiento Para El Desarrollo De Plantas Propulsivas Híbridas Limpias Y Eficientes A Través Del Uso De e-Fuels, entidad beneficiaria Universitat Politècnica de València.

6. Abbreviations

ATS	After-treatment system	LTC	Low temperature combustion
BAS	Belt Starter Assistance	MHEV	Mild hybrid electric vehicle
CAD	Crank Angle Degree	NHV	Noise, vibration, and harshness
CDC	Conventional diesel combustion	NOx	Nitrogen Oxides
DMDF	Dual-mode dual-fuel	OEM	Original equiment manufacturer
DOC	Diesel Oxidation Catalyst	OMEx	Oxymethylene dimethyl ether
DPF	Diesel Particle Filter	PFI	Port fuel injection
EGR	Exhaust gas recirculation	PHEV	Plug in electric vehicle
EM	Electric machine	RCCI	Reactivity Controlled Compression Ignition
EUVI	European Union emission limit six for heavy duty engines	REV	Range extender vehicle
HEV	Hybrid Electric Vehicle	SCR	Selective catalytic reduction
HRF	High reactivity fuel	SI	Spark Ignition
ICE	Internal Combustion Engine	SOC	State of the charge of the battery
LCA	Life cycle analysis	TM	Traction motor
LHV	Low heating value	TTW	Tank to wheel
LI-Ion	Litium Ion batteries	WTT	Well to tank
LRF	Low reactivity fuel	WTW	Well to wheel

7. References

[1] Taymaz I, Benli M. Emissions and fuel economy for a hybrid vehicle. Fuel 2014;115:812–7. doi:10.1016/j.fuel.2013.04.045.

[2] García A, Monsalve-serrano J, Sari RL, Martinez-boggio S. An optical investigation of thermal runway phenomenon under thermal abuse conditions. Energy Convers Manag 2021;246:114663. doi:10.1016/j.enconman.2021.114663.

[3] Fagundez JLS, Sari RL, Garcia A, Pereira FM, Martins MES, Salau NPG. A chemical kinetics based investigation on laminar burning velocity and knock occurrence in a spark-ignition engine fueled with ethanol–water blends. Fuel 2020;280:118587. doi:10.1016/j.fuel.2020.118587.

[4] Alvarez R, Weilenmann M. Effect of low ambient temperature on fuel consumption and pollutant and CO 2 emissions of hybrid electric vehicles in real-world conditions. Fuel 2012;97:119–24. doi:10.1016/j.fuel.2012.01.022.

[5] Wang Y, Wang J, Hao C, Wang X, Li Q, Zhai J, et al. Characteristics of instantaneous particle number (PN) emissions from hybrid electric vehicles under the real-world driving conditions. Fuel 2021;286:119466.

doi:10.1016/j.fuel.2020.119466.

[6] Duan H, Jia M, Chang Y, Liu H. Experimental study on the influence of low-temperature combustion (LTC) mode and fuel properties on cyclic variations in a compression-ignition engine. Fuel 2019;256:115907. doi:10.1016/j.fuel.2019.115907.

[7] Kokjohn SL, Hanson RM, Splitter DA, Reitz RD. Fuel reactivity controlled compression ignition (RCCI): a pathway to controlled high-efficiency clean combustion. Int J Engine Res 2011;12:209–26. doi:10.1177/1468087411401548.

[8] Benajes J, García A, Monsalve-Serrano J, Lago Sari R. Fuel consumption and engine-out emissions estimations of a light-duty engine running in dual-mode RCCI/CDC with different fuels and driving cycles. Energy 2018;157:19–30. doi:10.1016/j.energy.2018.05.144.

[9] García A, Monsalve-Serrano J, Martínez-Boggio S, Rückert Roso V, Duarte Souza Alvarenga Santos N. Potential of bio-ethanol in different advanced combustion modes for hybrid passenger vehicles. Renew Energy 2020;150:58–77. doi:10.1016/j.renene.2019.12.102.

[10] Benajes J, García A, Monsalve-Serrano J, Martínez-Boggio S. Optimization of the parallel and mild hybrid vehicle platforms operating under conventional and advanced combustion modes. Energy Convers Manag 2019;190:73–90. doi:10.1016/j.enconman.2019.04.010.

[11] Benajes J, García A, Monsalve-Serrano J, Sari R. Clean and efficient dual-fuel combustion using OMEx as high reactivity fuel: Comparison to diesel-gasoline calibration. Energy Convers Manag 2020;216:112953. doi:10.1016/j.enconman.2020.112953.

[12] Huang G, Li Z, Zhao W, Zhang Y, Li J, He Z, et al. Effects of fuel injection strategies on combustion and emissions of intelligent charge compression ignition (ICCI) mode fueled with methanol and biodiesel. Fuel 2020;274:117851. doi:10.1016/j.fuel.2020.117851.

[13] Luján JM, García A, Monsalve-Serrano J, Martínez-Boggio S. Effectiveness of hybrid powertrains to reduce the fuel consumption and NOx emissions of a Euro 6d-temp diesel engine under real-life driving conditions. Energy Convers Manag 2019;199:111987. doi:10.1016/j.enconman.2019.111987.

[14] García A, Monsalve-Serrano J, José Sanchís E, Fogué-Robles Á. Exploration of suitable injector configuration for dual-mode dual-fuel engine with diesel and OMEx as high reactivity fuels. Fuel 2020;280:118670. doi:10.1016/j.fuel.2020.118670.

[15] Solouk A, Shakiba-Herfeh M, Arora J, Shahbakhti M. Fuel consumption assessment of an electrified powertrain with a multi-mode high-efficiency engine in various levels of hybridization. Energy Convers Manag 2018;155:100–15. doi:10.1016/j.enconman.2017.10.073.

[16] García A, Monsalve-Serrano J, Sari R, Dimitrakopoulos N, Tunér M, Tunestål P.

Performance and emissions of a series hybrid vehicle powered by a gasoline partially premixed combustion engine. Appl Therm Eng 2019;150. doi:10.1016/j.applthermaleng.2019.01.035.

[17] García A, Monsalve-Serrano J, Martinez-Boggio S, Gaillard P, Poussin O, Amer AA. Dual fuel combustion and hybrid electric powertrains as potential solution to achieve 2025 emissions targets in medium duty trucks sector. Energy Convers Manag 2020;224:113320. doi:10.1016/j.enconman.2020.113320.

[18] Poussin O, Gaillard P, Garcia A, Monsalve-Serrano J, Martinez-Boggio SD. Dual-Fuel RCCI Diesel-Gasoline Hybrid Truck Concept to Achieve the Future Emissions Targets. 10th Aachen Colloq. China Sustain. Mobil. 2020, 2020.

[19] Ji C, Wang S, Zhang B, Liu X. Emissions performance of a hybrid hydrogen-gasoline engine-powered passenger car under the New European Driving Cycle. Fuel 2013;106:873–5. doi:10.1016/j.fuel.2013.01.011.

[20] Hanson R, Spannbauer S, Gross C, Reitz RD, Curran S, Storey J, et al. Highway Fuel Economy Testing of an RCCI Series Hybrid Vehicle. SAE Tech Pap Ser 2015;1. doi:10.4271/2015-01-0837.

[21] Warey A, Bucknor N, Sutherland I, Potter M. An Exploratory Assessment of Electrified Propulsion Systems for Full-Size Heavy-Duty Truck Applications. SAE Tech Pap Ser 2019;1:1–7. doi:10.4271/2019-01-5002.

[22] Kivekäs K, Lajunen A, Vepsäläinen J, Tammi K. City bus powertrain comparison: Driving cycle variation and passenger load sensitivity analysis. Energies 2018;11. doi:10.3390/en11071755.

[23] Zhu H, McCaffery C, Yang J, Li C, Karavalakis G, Johnson KC, et al. Characterizing emission rates of regulated and unregulated pollutants from two ultra-low NOx CNG heavy-duty vehicles. Fuel 2020;277:118192. doi:10.1016/j.fuel.2020.118192.

[24] García A, Gil A, Monsalve-Serrano J, Lago Sari R. OMEx-diesel blends as high reactivity fuel for ultra-low NOx and soot emissions in the dual-mode dual-fuel combustion strategy. Fuel 2020;275:117898. doi:10.1016/j.fuel.2020.117898.

[25] Vedachalam S, Boahene P, Dalai AK. Production of jet fuel by hydrorefining of Fischer-Tropsch wax over Pt/Al-TUD-1 bifunctional catalyst. Fuel 2021;300:121008. doi:10.1016/j.fuel.2021.121008.

[26] Bongartz D, Burre J, Mitsos A. Production of Oxymethylene Dimethyl Ethers from Hydrogen and Carbon Dioxide - Part I: Modeling and Analysis for OME1. Ind Eng Chem Res 2019;58:4881–9. doi:10.1021/acs.iecr.8b05576.

[27] Omari A, Heuser B, Pischinger S. Potential of oxymethylenether-diesel blends for ultra-low emission engines. Fuel 2017;209:232–7. doi:10.1016/j.fuel.2017.07.107.

[28] Rodríguez-Fernández J, Lapuerta M, Sánchez-Valdepeñas J. Regeneration of diesel particulate filters: Effect of renewable fuels. Renew Energy 2017;104:30–9. doi:10.1016/j.renene.2016.11.059.

[29] Bongartz D, Doré L, Eichler K, Grube T, Heuser B, Hombach LE, et al. Comparison of light-duty transportation fuels produced from renewable hydrogen and green carbon dioxide. Appl Energy 2018;231:757–67. doi:10.1016/j.apenergy.2018.09.106.

[30] Gamma Technologies. Vehicle_Driveline_and_HEV application manual 2016.

[31] García A, Monsalve-Serrano J, Lago Sari R, Gaillard P. Assessment of a complete truck operating under dual-mode dual-fuel combustion in real life applications: Performance and emissions analysis. Appl Energy 2020;279:115729. doi:10.1016/j.apenergy.2020.115729.

[32] Battery EE, Training M. GT-SUITE Electrical Equivalent Battery 2019.

[33] Colombo M, Nova I, Tronconi E. A comparative study of the NH3-SCR reactions over a Cu-zeolite and a Fe-zeolite catalyst. Catal Today 2010;151:223–30. doi:10.1016/j.cattod.2010.01.010.

[34] García A, Monsalve-Serrano J, Villalta D, Lago Sari R. Performance of a conventional diesel aftertreatment system used in a medium-duty multi-cylinder dual-mode dual-fuel engine. Energy Convers Manag 2019;184. doi:10.1016/j.enconman.2019.01.069.

[35] Guan B, Zhan R, Lin H, Huang Z. Review of the state-of-the-art of exhaust particulate filter technology in internal combustion engines. J Environ Manage 2015;154:225–58. doi:10.1016/j.jenvman.2015.02.027.

[36] Volvo. Volvo FE: Product Guide 2017:36.

[37] García A, Monsalve-Serrano J, Lago Sari R, Martinez-Boggio S. Energy assessment of an electrically heated catalyst in a hybrid RCCI truck. Energy 2022;238:121681. doi:10.1016/j.energy.2021.121681.

[38] García A, Carlucci P, Monsalve-Serrano J, Valletta A, Martínez-Boggio S. Energy management optimization for a power-split hybrid in a dual-mode RCCI-CDC engine. Appl Energy 2021;302:117525. doi:10.1016/j.apenergy.2021.117525.

[39] Northrop WF, Bohac S V., Chin JY, Assanis DN. Comparison of filter smoke number and elemental carbon mass from partially premixed low temperature combustion in a direct-injection diesel engine. J Eng Gas Turbines Power 2011;133. doi:10.1115/1.4002918.

[40] Benajes J, García A, Pastor JM, Monsalve-Serrano J. Effects of piston bowl geometry on reactivity controlled compression ignition heat transfer and combustion losses at different engine loads. Energy 2016;98:64–77. doi:10.1016/j.energy.2016.01.014.

[41] García A, Monsalve-Serrano J, Villalta D, Lago Sari R, Gordillo Zavaleta V, Gaillard P. Potential of e-Fischer Tropsch diesel and oxymethyl-ether (OMEx) as fuels for the dual-mode dual-fuel concept. Appl Energy 2019;253:113622. doi:10.1016/j.apenergy.2019.113622.

[42] Serrano JR, García A, Monsalve-Serrano J, Martínez-Boggio S. High efficiency two

stroke opposed piston engine for plug-in hybrid electric vehicle applications: Evaluation under homologation and real driving conditions. Appl Energy 2021;282:116078. doi:10.1016/j.apenergy.2020.116078.

[43] Translation from German original THE CONCEPT OF EFFICIENCY IN THE GERMAN CLIMATE POLICY DEBATE ON ROAD TRANSPORT A comprehensive approach to assessing the efficiency of technologies (translation from the German original version) 2020.

[44] Bouet A, Won HW, Morel V, Thirouard M, De Francqueville L, Noel L. Potential of Naphtha-like Fuel on an Existing Modern Compression Ignition Engine. SAE Tech Pap 2015;2015-Septe. doi:10.4271/2015-01-1813.

[45] Blanco H, Nijs W, Ruf J, Faaij A. Potential for hydrogen and Power-to-Liquid in a low-carbon EU energy system using cost optimization. Appl Energy 2018;232:617–39. doi:10.1016/j.apenergy.2018.09.216.

[46] Verhelst S, Turner JW, Sileghem L, Vancoillie J. Methanol as a fuel for internal combustion engines. Prog Energy Combust Sci 2019;70:43–88. doi:10.1016/j.pecs.2018.10.001.

[47] García A, Monsalve-Serrano J, Villalta D, Sari R. Octane number influence on combustion and performance parameters in a Dual-Mode Dual-Fuel engine. Fuel 2019;258. doi:10.1016/j.fuel.2019.116140.

[48] García A, Monsalve-Serrano J, Villalta D, Sari R. Fuel sensitivity effects on dual-mode dual-fuel combustion operation for different octane numbers. Energy Convers Manag 2019;201. doi:10.1016/j.enconman.2019.112137.

[49] Morel V, Francqueville L, Laget O, Malbec LM, Noel L. Potential of CN25 Naphtha-Based Fuel to Power Compression Ignition Engines. SAE Tech Pap 2016;2016-April. doi:10.4271/2016-01-0765.

[50] Poussin O, García A, Sari R, Gaillard P, Gordillo V. Dual-fuel RCCI OMEx-gasoline combustion to reduce the well-to- wheel CO 2 levels towards the 2025 horizon. SIA Powertrain, Energy Power Electron. Congr., 2020.

[51] Trucks V. Volvo FL Electric. Urban deliveries and waste collection n.d. https://www.volvotrucks.com/en-en/trucks/trucks/volvo-fl/volvo-fl-electric.html#spec.

[52] Scania. Scania’s new hybrid truck with 60 km electric range n.d. https://www.scania.com/group/en/home/newsroom/press-releases/press-release-detail-page.html/3768732-scania-s-new-hybrid-truck-with-60-km-electric-range.

[53] Guardiola C, Pla B, Bares P, Barbier A. Safe operation of dual-fuel engines using constrained stochastic control. Int J Engine Res 2021. doi:10.1177/1468087420985109.

[54] Heywood JB. Internal Combustion Engine Fundamentals. 2018.

[55] ACEA. ACEA Position Paper Views on proposals for Euro 7 emission standard

2020:18.

[56] Samaras Z, Hausberger S. Preliminary findings on possible Euro 7 emission limits for LD and HD vehicles. Online AGVES Meet 2020.

[57] García A, Monsalve-Serrano J, Lago Sari R, Gaillard P. Assessment of a complete truck operating under dual-mode dual-fuel combustion in real life applications: Performance and emissions analysis. Appl Energy 2020;279:115729. doi:10.1016/j.apenergy.2020.115729.

8. Appendix

Appendix A

Figure A1 shows the calibration maps for Diesel-Gasoline and OMEx-Gasoline for the 8L / 6 cylinders engine. The engine is calibrated up to 210 hp (60% of engine load) in full RCCI mode and DMDF up to 350 hp (100% of engine load). Brake specific: fuel mass consumption, fuel volume, CO_2 Tank-to-Wheel, CO_2 Well-to-Wheel, Premix Energy Ratio, NOx and Soot are presented.

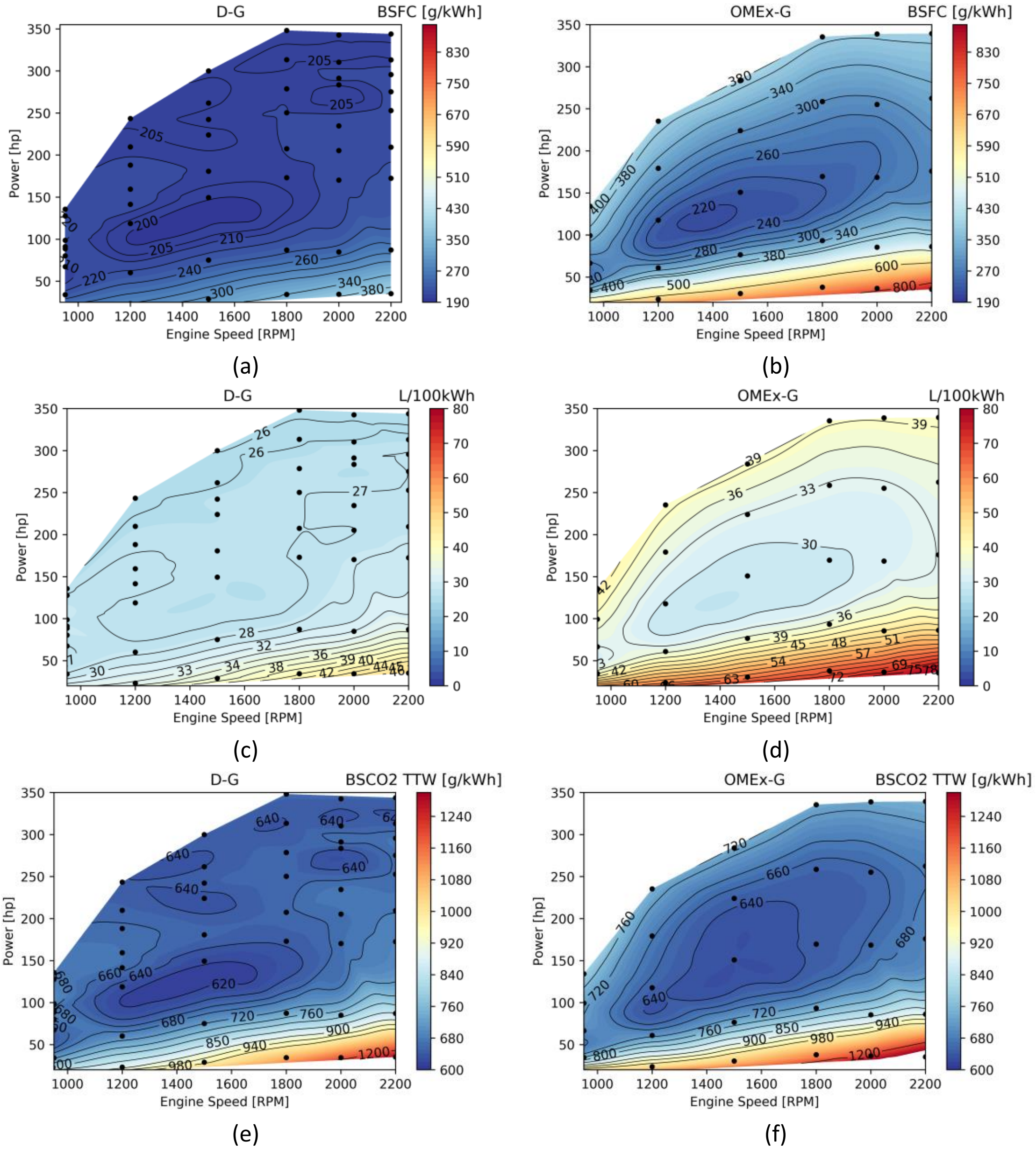

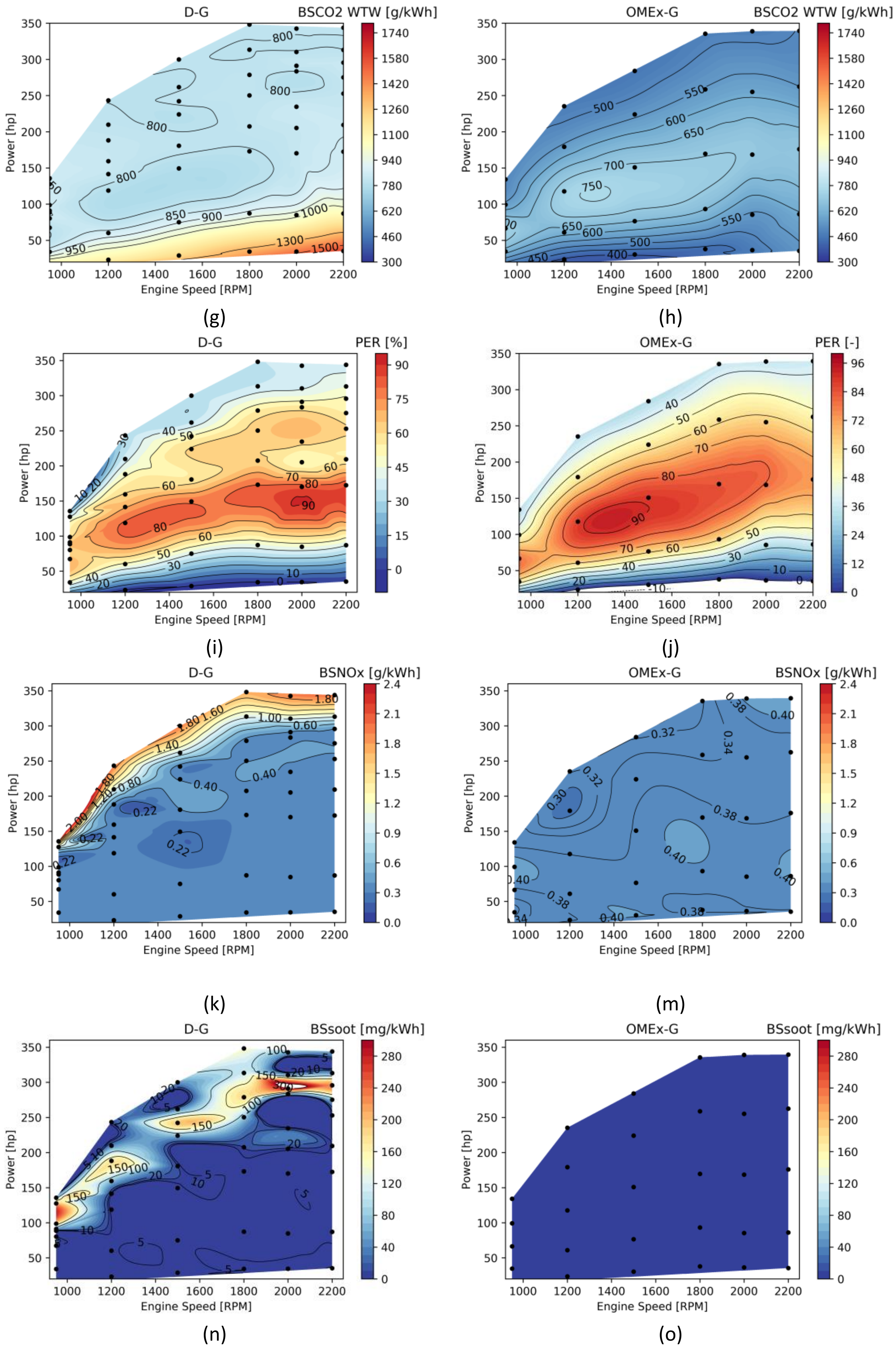

Figure A1- Engine calibration maps in terms of fuel consumption, premix energy ratio and emissions.

Appendix B

In this study, different driving cycles that represent homologation conditions, such as the WHVC, and real driving emissions are selected. The data to model the last-mentioned cycles was taken in real routes through a GPS in a no-hybrid commercial diesel Truck. The driving cycles selected for this study represent combined cycles with urban, rural and highway phases (Figure B1). Only Urban Hilly does not contain the highway phase. It is important to note that altitude measurements were considered in the real driving cycles. For the WHVC, the altitude is zero due to the homologation specifications. Moreover, the duration and total distance of the real driving conditions are larger than the WHVC. The most important cycle statistics can be found in Table B1.

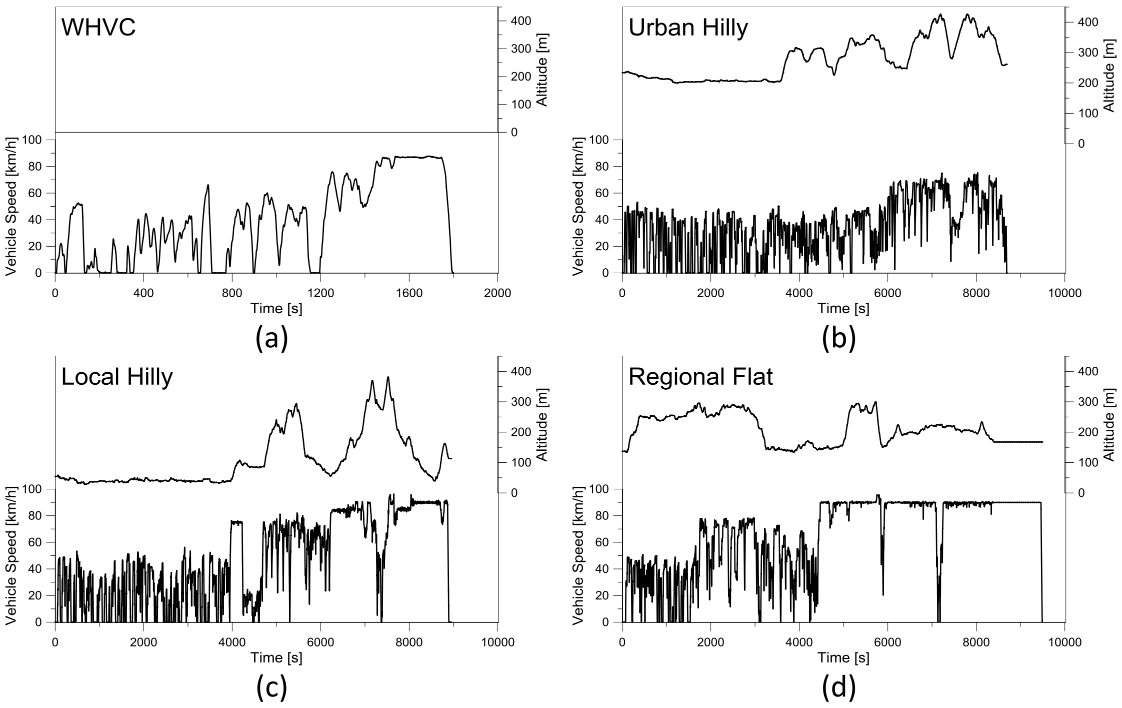

Figure B1- Homologation and real driving cycles with vehicle speed and altitude against time.

Table B1 – Driving cycle main characteristics

Parameter	**WHVC**	**Urban Hilly**	**Local Hilly**	**Regional Flat**
Time [min]	30	145	138	158
Distance [km]	20	85	119	176
Max Speed [km/h]	88	75	96	96
Avg Speed [km/h]	40	35	48	66
Acc time [%]	46	29	29	20
Dec time [%]	32	21	24	16
Stop time [%]	26	12	13	4
Cruising [%]	28	38	34	61
RPA [m/s^2]	0.09	0.12	0.10	0.06

Appendix C

A DoE is performed to optimize the battery size, differential ratio, and energy management system for the series hybrid with Diesel-Gasoline. The main results are depicted in Figure C1. It is important to note that the case of study selected for the optimization was the homologation driving cycle for heavy-duty vehicles at full payload. This last parameter was selected due to the challenging condition that is represented when the truck is completely loaded. In hybrid applications for HDV, it is well known that the fuel consumption benefits decrease with the increase of the payload due to the high efficiency of the conventional powertrain at high load conditions [17].

The optimum case (marked with a star) was found to be a battery size of 46 kWh (Figure a). The battery size has a negligible effect up to 30 kWh, with a decrease in terms of CO_2 emissions of 0.7% with respect to the minimum battery size tested (20 kWh) due to the decrease of the thermal losses. Then, the CO_2 reduction is maintained flat up to 50 kWh. Above from this value, the battery weight has a larger effect than the decrease of the heat losses in the cells and the CO_2 benefits decreases. The other hardware parameter optimized is the differential ratio, which changes the electric machine operation zone (low differential ratio implies lower EM rotational speed and higher torques, and high differential ratio implies the contrary). Figure C1 shows that the color bar in shades of blue is the best selection with an optimum value of 9.5. The high multiplication ratio increases the electric machine speed, improving the efficiency. The vehicle study in this work is submitted to low road speed. Therefore, the optimization confirms the benefits of increasing the speed and reducing the torque necessary in the EM. It is possible to see that the correct selection of the differential ratio is the most important factor. All cases above the OEM truck have a final drive below 6:1. Above 8:1 the trend is flat with small gains.

In terms of control strategy, the SOC width was found to have an optimum of 2.9% (Figure C1b). The SOC width has an important effect in the CO_2 benefits, with high benefits decreased above 4% of SOC width. This enhances the necessity of the DoE to correctly set the powertrain battery and calibration strategy. The maximum benefit in full payload under WHVC was 3.3% of CO_2 reduction. In spite of being far from the 2025 European target of 25% CO_2 reduction, the condition used to optimize is the most challenging for the studied application.

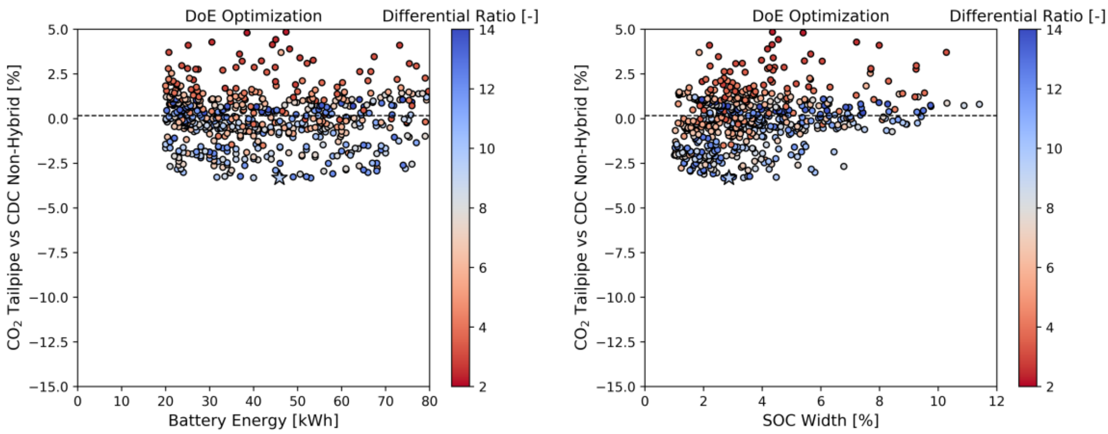

(a) (b)

Figure C1- DoE optimization results in terms of TTW CO_2 reduction for battery size (a) and SOC width (b) in the WHVC at 100% payload with Diesel-Gasoline calibration. The color bar shows the differential ratio range.